remote sensing

MDPI

Article

GloWS-Net: A Deep Learning Framework for Retrieving Global Sea Surface Wind Speed Using Spaceborne GNSS-R Data

Jinwei Bu [1,2], Kegen Yu [2,*], Xiaoqing Zuo [1], Jun Ni [3], Yongfa Li [1] and Weimin Huang [4]

[1] Faculty of Land Resources Engineering, Kunming University of Science and Technology, Kunming 650093, China
[2] School of Environment Science and Spatial Informatics, China University of Mining and Technology, Xuzhou 221116, China
[3] School of Information Science and Engineering, Yunnan University, Kunming 650500, China
[4] Department of Electrical and Computer Engineering, Memorial University of Newfoundland, St. John's, NL A1B 3X5, Canada
* Correspondence: kegen.yu@cumt.edu.cn

Abstract: Spaceborne Global Navigation Satellite System Reflectometry (GNSS-R) is a new remote sensing technology that uses GNSS signals reflected from the Earth's surface to estimate geophysical parameters. Because of its unique advantages such as high temporal and spatial resolutions, low observation cost, wide coverage and all-weather operation, it has been widely used in land and ocean remote sensing fields. Ocean wind monitoring is the main objective of the recently launched Cyclone GNSS (CYGNSS). In previous studies, wind speed was usually retrieved using features extracted from delay-Doppler maps (DDMs) and empirical geophysical model functions (GMFs). However, it is a challenge to employ the GMF method if using multiple sea state parameters as model input. Therefore, in this article, we propose an improved deep learning network framework to retrieve global sea surface wind speed using spaceborne GNSS-R data, named GloWS-Net. GloWS-Net considers the fusion of auxiliary information including ocean swell significant wave height (SWH), sea surface rainfall and wave direction to build an end-to-end wind speed retrieval model. In order to verify the improvement of the proposed model, ERA5 and Cross-Calibrated Multi-Platform (CCMP) wind data were used as reference for extensive testing to evaluate the wind speed retrieval performance of the GloWS-Net model and previous models (i.e., GMF, fully connected network (FCN) and convolutional neural network (CNN)). The results show that, when using ERA5 winds as ground truth, the root mean square error (RMSE) of the proposed GloWS-Net model is 23.98% better than that of the MVE method. Although the GloWS-Net model and the FCN model have similar RMSE (1.92 m/s), the mean absolute percentage error (MAPE) of the former is improved by 16.56%; when using CCMP winds as ground truth, the RMSE of the proposed GloWS-Net model is 2.16 m/s, which is 20.27% better than the MVE method. Compared with the FCN model, the MAPE is improved by 17.75%. Meanwhile, the GloWS-Net outperforms the FCN, traditional CNN, modified CNN (MCNN) and CyGNSSnet models in global wind speed retrieval especially at high wind speeds.

Keywords: Cyclone Global Navigation Satellite System (CYGNSS); delay-Doppler maps (DDMs); ocean wind speed; geophysical model functions (GMFs); deep learning

Citation: Bu, J.; Yu, K.; Zuo, X.; Ni, J.; Li, Y.; Huang, W. GloWS-Net: A Deep Learning Framework for Retrieving Global Sea Surface Wind Speed Using Spaceborne GNSS-R Data. *Remote Sens.* **2023**, *15*, 590. https://doi.org/10.3390/rs15030590

Academic Editors: Hugo Carreno-Luengo, Dallas Masters and Chun-Liang Lin

Received: 16 November 2022
Revised: 13 January 2023
Accepted: 17 January 2023
Published: 18 January 2023

1. Introduction

Ocean wind speed is of great significance for the numerical prediction of the marine environment, monitoring of marine disasters, air sea interaction, meteorological forecasting, climate research, etc. In particular, tropical cyclones, typhoons or storm surges have seriously damaged infrastructure and endangered people's lives. For these reasons, it is very important to monitor the sea wind speed to study and predict some complex weather (such as tropical cyclone, typhoon or storm surge warning) [1–3]. Long-term measurements of ocean wind speed can be made using conventional observational methods such

as buoys and ships. However, due to less spatial sampling and high cost, they cannot meet the needs of global observation. At present, there are two main ways for observing the sea surface wind field through satellite. One is to measure the sea wind through satellite cloud images, but it only obtains the cloud top wind, which is different from the sea surface wind field; second, the satellite load, such as the scatterometer, actively transmits microwave signals to the sea surface to measure the sea breeze. However, the satellite weight is large, and it can only measure the sea breeze within 50 m/s. If it is applied to the construction of constellations for quasi real-time monitoring of the sea wind field, the cost is very high. Although many monitoring and early warning systems have been established worldwide, it is also important to use GNSS to achieve an effective and cost-effective approach to disaster monitoring. Therefore, the spaceborne GNSS-R technology can provide a more effective alternative for ocean wind speed retrieval because of its remarkable advantages such as rich signal sources, high resolution, all-weather, and global fast coverage, etc. At present, many disaster monitoring systems using GNSS signals have been developed. For example, on 8 July 2014, the United Kingdom launched the TechDemoSat-1 (TDS-1) satellite [4]. In December 2016, National Aeronautics and Space Administration (NASA) successfully deployed the Cyclone Global Navigation Satellite System (CYGNSS) composed of eight small satellites, bringing greater opportunities for retrieving sea surface wind speed using GNSS-R technology [5]. More fortunately, BuFeng-1 A/B dual satellites were launched on 5 June 2019, which is China's first GNSS-R satellite mission dedicated to GNSS-R applications. China has become the fourth country after the United Kingdom, the United States and Japan to install GNSS-R satellites in the Earth's orbit. At the same time, BF-1 A/B is the only two GNSS-R constellations in the world. The mission also acquired the world's first on-board BDS DDM [6]. In addition to BF-1 A/B satellites, China also launched FengYun-3E meteorological satellite on 5 July 2021. The GNSS-R data observed by the satellite have been used for the retrieval of sea surface wind speed [7]. In addition, the satellite mission is also committed to GNSS radio occultation (GNSS-RO)-related applications. It is worth mentioning that although the main objective of the above spaceborne GNSS-R tasks is to monitor ocean wind speed, these satellite tasks can also be used for sea surface height retrieval [8,9], sea ice detection [10,11], sea ice concentration (SIC) retrieval [12,13], sea ice thickness retrieval [14], tsunami detection [15], storm surge monitoring [16,17], wave height retrieval [18–24], rainfall detection [25,26], rainfall intensity retrieval [27,28], soil moisture retrieval [29] and biomass retrieval [30], etc.

For the spaceborne platform, Clarizia et al. proposed to use the DDM average (DDMA), DDM variance (DDMV), DDM Allan variance (DDMAV), leading edge slope (LES) and trailing edge slope (TES) observables to retrieve wind speed [31]. Although the use of multiple observables has enriched the data information, it increases the computation load of the algorithm. Ruf et al. developed parametric models for high and low wind speeds using the normalized bistatic radar cross section (NBRCS) of the sea surface and the LES. Through a thorough evaluation of wind speed retrieval performance of geophysical model functions (GMF) by the NBRCS and LES methods, the overall root mean square (RMS) uncertainty of wind speed retrieved by CYGNSS has been found to be 1.4 m/s [32]. At high wind speed, the increased retrieval error is mainly due to the decrease in the sensitivity of the ocean scattering section to wind speed change. Clarizia and Ruf proposed a retrieval algorithm for the level 2 sea surface wind speed data product of CYGNSS mission [33]. This algorithm combines the DDMA and LES wind speed estimates into an optimal weighted estimator based on the method described by Clarizia et al. in 2014. Due to the limitation of cumulative time and resolution, this algorithm is only applicable to two specific observables (DDMA and LES) [31]. In [34], the generalized observation (defined as the linear combination of DDM samples) was optimized by using three different methods (i.e., minimum wind speed variance, maximum signal to noise ratio and principal component analysis (PCA)). The results show that PCA has the best performance. Guo et al. proposed a sea surface wind speed retrieval method for spaceborne GNSS-R based on the particle swarm optimization (PSO) algorithm. The experimental results show that the retrieval

accuracy of the PSO method is superior to the classical MVE method. Hammond et al. used the spaceborne Galileo and BDS GNSS-R data collected by the UK TechDemoSat-1 mission to assess the geophysical sensitivity for the first time [35]. Unfortunately, due to the limited amount of reflective BDS data currently available, it is impossible to conduct a comprehensive analysis of the geophysical sensitivity of BDS signals. This research shows the possibility of wind speed retrieval and sea ice detection using spaceborne GNSS-R to acquire different GNSS reflection signals (such as GPS, Galileo and BDS) in the future. Liu et al. proposed a machine learning (ML) method for the retrieval of sea surface wind speed based on a multi hidden layer neural network (MHL-NN). The results show that MHL-NN method is superior to other methods in terms of root mean square error (RMSE) and mean absolute percentage error (MAPE). The method mainly takes DDMA and LES observables as input variables [36]. With the rapid development of artificial intelligence, the machine learning algorithm has been applied to spaceborne GNSS-R wind speed retrieval [36–43], and results with high accuracy have been obtained. In recent years, some researchers have proposed and improved the calculation method of NBRCS [44–46]. Combined with power calibration, NBRCS can be calculated more accurately, to obtain better retrieval results, so it can be consistent with the entire sea surface wind speed range. Based on the DDM data obtained by Bufeng-1 satellite, Jing et al. developed an empirical geophysical function model using the NBRCS observable. Preliminary tests showed that the RMSE between the results obtained by the model and the ECMWF reanalysis wind speed was 2.63 m/s, and the determination coefficient was 0.55. Bu et al. proposed a combined wind speed retrieval model using both the NBRCS and LES observables [47]. The RMSE and determination coefficient of the combined method is 2.1 m/s and 0.906, respectively. Compared with the single-observable model based on NBRCS or LES, it achieves considerable performance improvement.

Table 1 summarizes the comparison of methods for spaceborne GNSS-R sea surface wind speed (WS) retrieval, mainly from the aspects of retrieval methods, GNSS-R observables, retrieval models and retrieval accuracy. Only representative literature is listed in the table, and "-" means not involved. Among them, MHL-NN represents a multi hidden layer neural network, ANN means an artificial neural network, HMDL denotes a heterogeneous multi-mode deep learning network, CNN means a convolutional neural network, MCNN indicates a statistically modified CNN and FA-RDN represents a cyclic neural network of feature attention mechanisms. It can be seen from Table 1, for the GMF method, some features (e.g., LES, TES and normalized bistatic radar cross section (NBRCS)) related to sea surface wind speed are extracted from DDM first. Next, by fitting an empirical function that links DDM observables with wind speed, and linear regression is applied to build GMF, then the minimum variance estimator (MVE) is used to combine the retrieval results of single observables and eliminate the residuals [31]. Although, the MVE method can achieve an accuracy of about 2 m/s for wind speed in the range of 0–30 m/s. However, the accuracy improvement of the MVE method over a single observable based method is still limited. Further research shows that the GNSS-R wind retrieval can be affected by incidence angle, reflection geometric parameters (such as longitude and latitude of specular point) [42,48] and sea conditions (such as significant wave height). Ocean swell caused by non-local winds may also have an impact on sea surface roughness [41,49,50], especially at very low wind speeds. It is difficult to develop a joint model through an analytical approach while considering all the factors. Therefore, in the traditional algorithm development, only a limited set of observations and features are used, which limits the accuracy of wind speed retrieval. However, it is encouraging that the GNSS-R wind speed retrieval algorithm has been significantly improved in recent years, opening a window for retrieving global wind speed from spaceborne GNSS-R data. In particular, the algorithm based on deep learning has been used to measure global ocean wind speed and achieved satisfactory results from spaceborne GNSS-R data [40–42]. Deep learning provides the ability to mitigate the impact caused by interfering data. However, due to the uneven distribution of wind speed samples, the retrieval performance of the deep learning model for high wind

speeds is poor. Therefore, samples in a wider wind speed range should be selected for a more generally applicable spaceborne GNSS-R wind speed retrieval model.

Table 1. Comparison of spaceborne GNSS-R sea surface wind speed retrieval methods.

Methods	Literature	GNSS-R Observables	Retrieval Models	Retrieval Accuracy
Waveform matching method	[51]	Normalized power value of DDM	-	1–2 m/s for WS < 20 m/s
Empirical model method	[31,33,34,47,52–54]	DDMA, DDMAV, ADDMV, LES, TES, NBRCS, Generalized Linear Observables	Polynomial fitting, exponential function, power function, combination of multiple observables.	~2 m/s for WS < 20 m/s
Intelligent optimization algorithm	[31,55]	NBRCS 、 LES	Combination model based on MVE and PSO.	PSO method is better than MVE method. The RMSE is better than 1.95 m/s for WS < 20 m/s.
Machine/Deep learning method	[36,38–43]	DDM, DDMA, LES, incidence angle, NBRCS, GPS satellite number, RCG, longitude and latitude of specular point, etc.	MHL-NN, ANN, HMDL, CNN, MCNN, FA-RDN	The retrieval accuracy of CNN, MCNN and FA-RDN models is the best. When the WS is less than 20-30 m/s, they are better than 1.36 m/s, 1.53 m/s and 1.45 m/s, respectively.

To solve the problem that the accuracy of wind speed retrieval of the empirical combination model is limited, the fully connected network (FCN) is applied to develop a multi feature wind speed retrieval model [37–43]. However, the improvement is mainly for the wind speed of 5–10 m/s because most data used are in this range. Due to overfitting, the estimated RMSE is much larger when it is above 15 m/s. Recently, Chu et al. used the one-month long TDS-1 data set to develop a more advanced architecture and proposed a multimodal deep learning model that fuses 34 auxiliary parameters with the DDM features extracted by CNN. The results show that the proposed model is substantially improved compared with FCN [39]. Asgarimehr and Guo et al. also applied multimodal CNN to the CYGNSS data and achieved decent performance [40,41]. Although these models are still affected by the probability density distribution function of wind speed, they open up a new prospect for GNSS-R wind speed inversion through a heterogeneous multimodal deep learning (HMDL) method.

In this paper, we propose an improved deep learning framework (i.e., GloWS-Net) for global sea surface wind speed retrieval from spaceborne GNSS-R data. GloWS-Net considers the fusion of auxiliary information (ocean swell SWH, sea surface rainfall and wave direction) to build an end-to-end wind speed retrieval model. Compared with previous methods, the proposed model has the following advantages:

(1) GloWS-Net includes a convolution layer for extracting effective features from the combination of BRCS DDM and corresponding effective scattering area, and a full connection layer for processing auxiliary parameters and higher-level input parameters. The best architecture is obtained based on the validation set and evaluated on the testing set to verify the generality of the model.
(2) When training GloWS-Net, some traditional machine learning strategies are used to prevent overfitting, including batch normalization and early stop.
(3) Contribution from different inputs is exploited by the GloWS-Net deep learning model. Meanwhile, the influence of swell and rainfall on wind speed retrieval performance is considered and corrected.
(4) The GloWS-Net model architecture has significantly reduced the underestimation phenomenon for high wind speeds. It outperforms the CyGNSSnet and MCNN architectures.

The rest of this paper is arranged as follows. Section 2 describes the data sets used and the basic modeling methods. Section 3 focuses on the design, training and validation of the GloWS-Net model. Section 4 compares the wind speed retrieval performance of different modeling methods, and discusses the results in detail. Section 5 provides the conclusion of this paper.

2. Data Set and Method Description

2.1. Data Set

To develop and test the retrieval model of the spaceborne GNSS-R sea surface wind speed, in this paper, six different data sets are used, including the CYGNSS GNSS-R L1 level data, ERA5 wind speed data, ERA5 swell significant wave height (SWH), ERA5 wave direction data, IMERG rainfall data, and the Cross-Calibrated Multi-Platform (CCMP) analysis wind (v02.1 near real time) products produced by Remote Sensing Systems (RSS). These data cover all the days of 2021.

(1) CYGNSS GNSS-R L1 level data

At present, the National Aeronautics and Space Administration (NASA) mainly provides users with three levels of CYGNSS GNSS-R data for free. The L1 level data product of version V3.1 is used in this article. This version mainly includes GNSS-R data from August 1, 2018 (DOY 213) to December 20, 2022. We can access the GNSS-R data from the website (https://podaac.jpl.nasa.gov/dataset/CYGNSS_L1_V3.1 (accessed on 19 December 2022)). This type of data records the DDM, specular point coordinates, transmitter positions and other relevant information of eight CYGNSS satellites (i.e., CY01, CY02, CY03, CY04, CY05, CY06, CY07 and CY08). In addition, CYGNSS L1 V3.1 also provides multiple DDM products (such as brcs, raw_counts, and power_analog). This article uses brcs and power_analog together with the effective scanning area corresponding to brcs.

(2) ERA5 reanalysis data sets

The Copernicus climate change service (C3S) climate database provides users with ECMWF reanalysis data products. ERA5 is the fifth generation atmospheric reanalysis of global climate by ECMWF. The reanalysis data combine the model data with the observation data from all over the world to form a global complete and consistent data set. ERA5 replaces its predecessor ERA Interim reanalysis. ERA5 contains multiple types of data sets. In this paper, we use ERA5 hourly data on a single level from 1959 to present (https://cds.climate.copernicus.eu/cdsapp#!/dataset/reanalysis-era5-single-levels (accessed on 1 July 2022)), which includes the data of 2 m temperature, 2 m dewpoint temperature, total precipitation, average sea level pressure, surface pressure, 10 m u-component of wind, 10 m v-component of wind, boundary layer height and sea surface wave height. We used ERA5 swell height data, ERA5 wave direction data, ERA5 10 m u-component of wind and 10 m v-component of wind data. Among them, the ERA5 swell height data represent the significant height of total swell. The 10 m u-component of wind and 10 m v-component of wind data are matched with other data through bilinear interpolation in space and linear interpolation in time. It should be noted that both the cubic and bilinear interpolation methods can be applied for matching data in a spatial domain, the bilinear method is usually used in the GNSS-R field. Since the results difference between them is negligible, the bilinear method is chosen here. Then, wind synthesis is conducted, and the resultant wind speed is used as the reference value of the real sea surface wind speed at 10 m above the sea surface. It is worth mentioning that the spatial resolution of ERA5 swell height data and ERA5 wave direction data is $0.5^\circ \times 0.5^\circ$ and temporal resolution is 1 h. However, the spatial resolution of 10 m u-component of wind and 10 m v-component of wind data is $0.25^\circ \times 0.25^\circ$ and temporal resolution is 1 h.

(3) Integrated Multi-satellite Retrievals for Global Precipitation Measurement (GPM IMERG) precipitation data sets

The Integrated Multi-satellite Retrievals for GPM (IMERG) algorithm combines information from the GPM satellite constellation to estimate precipitation over the majority of the Earth's surface. This algorithm is particularly valuable over the majority of the Earth's surface that lacks precipitation measuring instruments on the ground. Now in the latest Version 06 release of IMERG, the algorithm fuses the early precipitation estimates collected during the operation of the TRMM satellite (2000–2015) with more recent precipitation estimates collected during the operation of the GPM satellite (2014–present). GPM-IMERG has three types of products, namely IMERG Early Run (IMERG-E) (real-time products with a delay of about 4 h), IMERG Late Run (IMERG-L) (near real-time processing with a delay of about 14 h) and IMERG Final Run (IMERG-F). The spatial resolution of three types of products is $0.1^\circ \times 0.1^\circ$, they all have 1 month, 1 day and 30 min temporal resolutions. This article uses an IMERG-F product with a temporal resolution of 30 min, which can be downloaded from the GPM website for free (https://gpm.nasa.gov/data/directory (accessed on 1 July 2022)).

(4) RSS CCMP wind analysis product

The CCMP wind product was also used to evaluate the performance of the proposed model in retrieving wind speed. The CCMP is a combination of ocean surface (10 m) wind speed retrievals from multiple types of satellite microwave sensors and a background field from reanalysis. That is, CCMP simultaneously integrates multi-satellite sea surface winds of scatterometers from QuikSCAT and METOP-A/ASCAT, radiometers from SSM/I, SSMIS, AMSR, TMI, WindSat and GMI as well as in situ observations from NDBC, TAO, TRITON, RAMA, PIRATA and Canadian [56,57]. This data set has its own unique characteristics. CCMP wind data including u- and v-components were downloaded from Remote Sensing Systems (https://data.remss.com/ccmp/ (accessed on 19 December 2022)). The spatial resolution of its 10 m u-component of wind and 10 m v-component of wind data is $0.25^\circ \times 0.25^\circ$ and temporal resolution is 6 h. The coverage range is (0, 360°) for longitude and (−78.375°, −78.375°) for latitude. Wind speed at 10 m (U10) was calculated after respective interpolation of u and v wind components, which was used as the ground truth wind speeds.

Please note that in consideration of the spatial and temporal resolution difference between the CYGNSS GNSS-R data and ERA5 data set, CCMP wind data and IMERG rainfall data set, these data must be matched with the real sea surface ERA5 wind speed data at 10 m above the sea surface. Linear interpolation in time and bilinear interpolation in space are implemented to obtain the co-located sea surface wind speed.

2.2. Method Description

The data processing flow and model building process of the spaceborne GNSS-R sea surface wind speed retrieval method are shown in Figure 1. First, the CYGNSS DDM data are down sampled and spatially matched with the ERA5 wind speed, ERA5 wave direction, ERA5 swell SWH and IMERG rainfall data to produce the matched data set. To ensure the quality of the data set, the sampling data need to be quality controlled and filtered according to the standards listed in [24,28,42], so as to obtain the filtered high-quality data set. Then, the data set is randomly divided into training set, verification set and test set. They account for 30%, 15% and 55% of the filtered data set, respectively. The training set is used to train the model and the verification set is used to evaluate the performance of the network configuration. The content of network configuration is described in detail in Section 3.2. In the model training stage, it is necessary to specify the number of hidden layers and the number of neurons in each layer, and select the configuration with the best performance for the ultimate retrieval of global ocean wind speed.

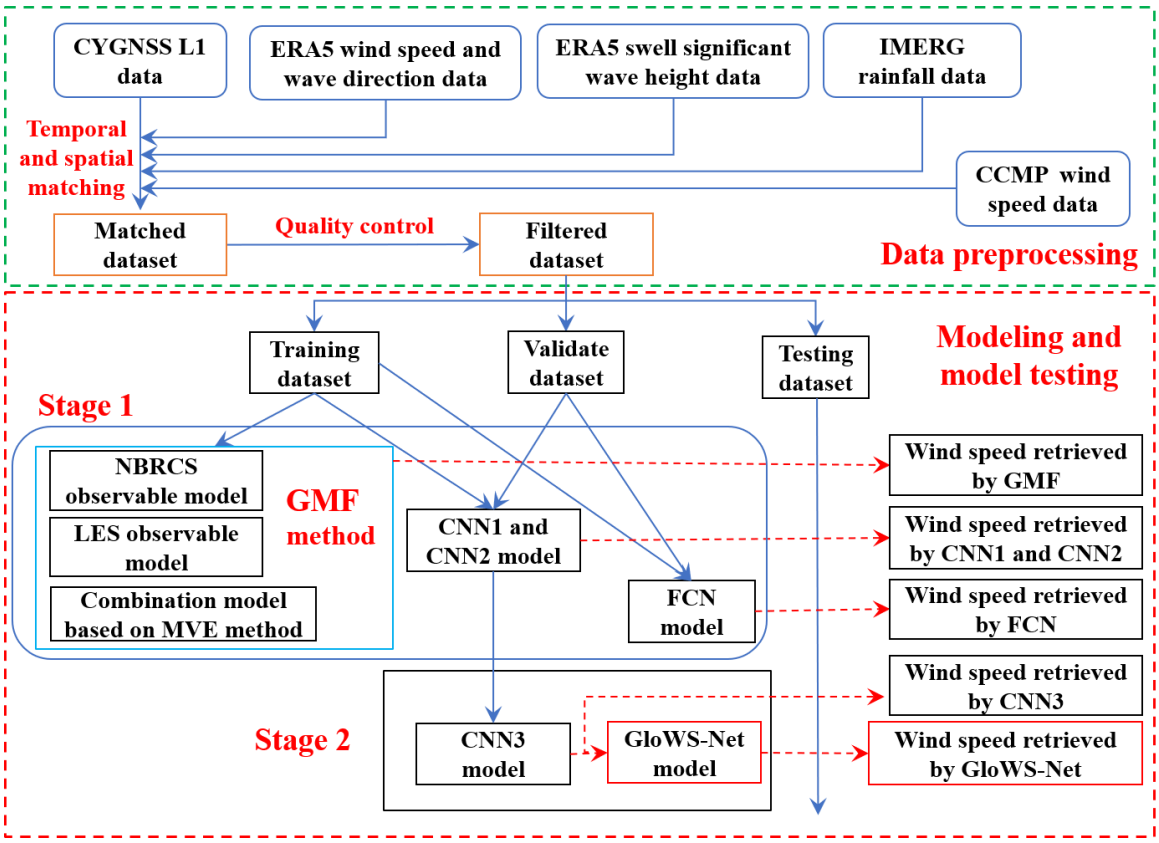

Figure 1. Data processing and model development process of spaceborne GNSS-R sea surface wind speed retrieval.

In order to confirm the improvement of the proposed model, the training model is further divided into two stages, namely the first stage and the second stage indicated by the red dotted box in Figure 1. In the first stage, the training set is used to establish the GMF, FCN and CNN models, and the latter two use the early stop method through the verification set to avoid overfitting. It should be noted that the ERA5 swell SWH, IMERG rainfall data and ERA5 wave direction data are not used to retrieve wind speed based on the GMF method. In this paper, the FCN models are divided into FCN1, FCN2, FCN3 and FCN4 models according to the number of input parameters in the input layer. The CNN models only have DDM images as input. According to the different types of DDM images, the CNN models are divided into CNN1 and CNN2 models (see Table 3 below). In the second stage, the CNN3 model is established by adding effective scattering area and additional auxiliary parameters corresponding to BRCS DDM on the basis of the CNN1 model. Please note that the CNN1, CNN2, CNN3 and GloWS-Net models are independent, and they are directly trained by the training set and supervised by the verification set. The CNN3 model is only designed to analyze the impact of introducing additional auxiliary parameters. For convenience, the proposed improved CNN model is named GloWS-Net model, and its retrieved wind speed is hereinafter referred to as GloWS-Net wind speed. Finally, the performance of these four models (GMF, CNN1, CNN2 and FCN) in the first stage and two models (CNN3 and GloWS-Net) in the second stage are tested on the test set. The reference wind speed data in the test set include the ERA5 and CCMP wind speed data, among which, the CCMP wind speed data are not used for model training, so this data set can better evaluate the robustness and generality of the proposed model. Details of each stage are provided later.

3. Development of the GloWS-Net Deep Learning Model

3.1. CYGNSS Observations and Other Auxiliary Observations

DDM is the basic data recorded by a GNSS-R receiver and also the most useful data. For the retrieval of sea surface wind speed using spaceborne GNSS-R technology, the peak value of bistatic reflected power will change, and the shape of the delayed Doppler maps will also change due to the variation in sea surface roughness. In the case of bistatic scattering, the relationship between wind speed and the peak DDM power is different from that of the backscattering geometry. When wind speed is low, the strong forward reflection will cause the received signal to be very strong. With the increase in wind speed, the peak power decreases. This is consistent with the situation observed in the DDM diagram under different wind speed conditions shown in Figure 2. It can be seen that the DDM of the GNSS signal reflected from the sea surface is horseshoe shaped, and the power value is usually the largest at the specular point. These differences provide a valuable opportunity for retrieving the sea surface wind speed based on spaceborne GNSS-R. Therefore, four variables (NBRCS, LES, TES and SNR) extracted from DDM have strong correlation with wind speed [58,59]. These variables are calibrated in the CYGNSS Level 1B product, which is usually used for wind speed retrieval [33]. The signal to noise ratio (SNR) is also strongly correlated with sea surface roughness [34,35]. NBRCS and LES are the two most important observables in CYGNSS products, which are very effective for wind speed retrieval. TES is the slope of the trailing edge of the integrated delay waveform, which is also useful for sea surface wind speed [31]. Please note that the TES observation value in this paper is calculated from the power DDM. In addition, this paper also uses two main measurement products, BRCS DDM and its corresponding effective scattering area. BRCS DDM has a size of 17 × 11, which is different from power DDM.

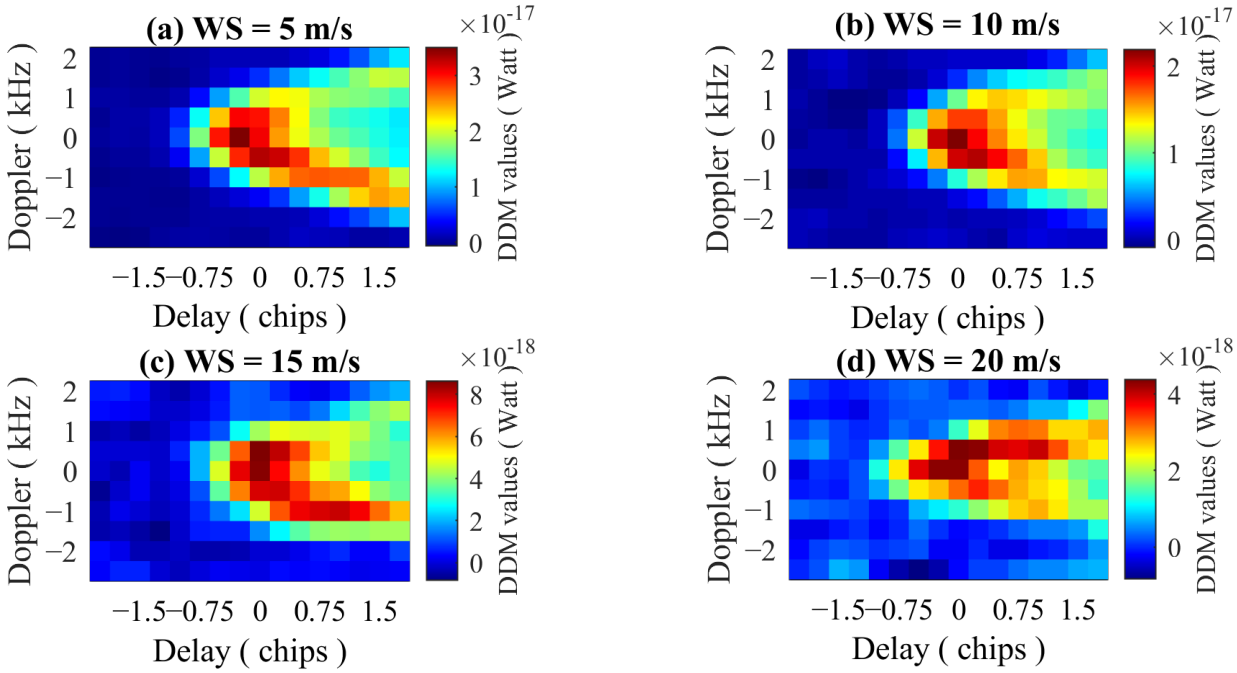

Figure 2. DDMs under different wind speed (WS) conditions.

In addition to the above observables, several other variables related to receiver, satellite geometry, sea state factors and weather conditions are also considered to improve the performance of the model. The receiver antenna gain reflects the state of signal reception, and the incident angle and specular reflection point describe the satellite geometry. Sea state factors mainly include swell and wave development degree will increase the uncertainty of spaceborne GNSS-R wind speed retrieval. For example, the wind speed retrieval in CYGNSS L2 is based on two independent GMFs (i.e., one for fully developed

sea and one for developing sea), taking into account the development of the ocean [54]. The GMF used by NOAA for CYGNSS wind speed retrieval includes SWH as the input parameter [60,61]. Li and Guo et al. also used swell SWH as input parameter to establish their wind speed retrieval model [41,42]. The swell is a long wave. The SWH of the swell will affect the GNSS signal reflection, so it is used as one input parameter. Similarly, this paper also uses SWH as a prior knowledge to improve the performance of the wind speed retrieval model. Secondly, because the sea wave information has an important contribution to wind speed retrieval based on the deep learning network, it is also helpful to use more sea wave related parameters as the input of the neural network training. However, considering that the structure complexity of the network and the computational load of the network training will increase significantly, which will affect the convergence of the training, the SWH of the swell and the wave direction parameters are mainly considered in the GloWS-Net model. In addition, rainfall will also affect the retrieval of spaceborne GNSS-R wind speed, especially at low wind speeds (<10 m/s), rainfall will lead to wind speed retrieval deviation [25,61,62], and wind speed deviation will increase with the increase in rainfall [61]. In order to consider the effect of rain, rainfall intensity is also added as an input parameter. For clarity, Table 2 lists the auxiliary parameters used in the GloWS-Net model.

Table 2. Specific description of input auxiliary parameters information of GloWS-Net model.

	Input Variables	Description
Related to DDM	NBRCS	Normalized bistatic radar cross section
	LES	Leading edge slope
	TES	Trailing edge slope
	SNR	DDM signal to noise ratio
Related to receiver	sp_rx_gain	Range corrected gain
Related to satellite geometry	sp_lon	Specular point longitude
	sp_lat	Specular point latitude
	sp_inc_angle	Specular point incidence angle
Other parameters	Swell SWH	ERA5 swell SWH
	Wave direction	ERA5 wave direction
	Rainfall intensity	IMERG rainfall intensity

3.2. GloWS-Net Model Design

In this section, we describe the general architecture of GloWS-Net (as shown in Figure 3) and the scheme for optimizing the network.

Please note that the GloWS-Net architecture proposed in this paper is different from the network architecture of Asgarimehr and Guo et al. [40,41]. In Figure 3, the GloWS-Net architecture has three input ports, the first for BRCS DDM, the second for effective scattering area and the third for auxiliary parameters. In particular, the third port inputs the longitude and latitude, incidence angle, NBRCS, LES, TES, rainfall information and other auxiliary variables of the specular reflection point. It can be seen from Figure 3 that the size of the characteristic map gradually decreases through the processing of different layers, and the results (i.e., wind speed) are finally output through the full connecting layer.

To compare with the GloWS-Net architecture proposed here, we provide the results of CNN1 architecture with only BRCS DDM input and CNN2 architecture with only power DDM input, and the results of FCN1, FCN2, FCN3 and FCN4 architectures with only auxiliary parameters but no convolution layer. These architectures are different in terms of auxiliary parameters and input image types. Information about architectures and auxiliary parameters is shown in Table 3.

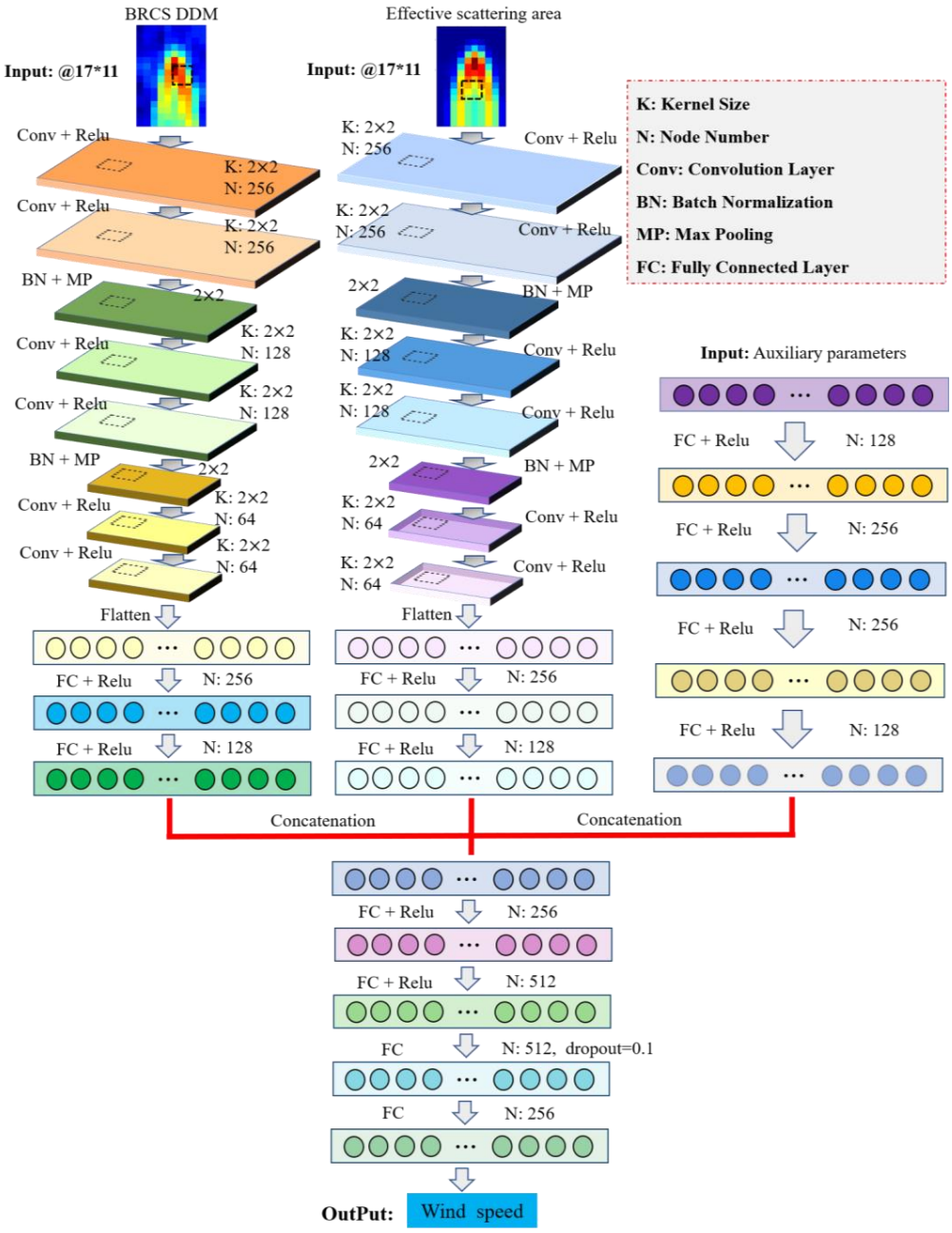

Figure 3. Architecture of GloWS-Net.

Table 3. Input parameters of FCN, CNN and GloWS-Net models.

Architecture (Model)	Input Image	Input Auxiliary Parameters (Variables)
FCN1	No	NBRCS, LES
FCN2	No	NBRCS, LES, TES, SNR, incidence angle, receiver antenna gain
FCN3	No	NBRCS, LES, TES, SNR, incidence angle, receiver antenna gain, longitude and latitude of specular point
FCN4	No	NBRCS, LES, TES, SNR, incidence angle, receiver antenna gain, longitude and latitude of specular point, swell SWH, wave direction, rainfall intensity
CNN1	BRCS DDM	No
CNN2	power_analog	No

Table 3. *Cont.*

Architecture (Model)	Input Image	Input Auxiliary Parameters (Variables)
CNN3	BRCS DDM, effective scattering area	NBRCS, LES, TES, SNR, incidence angle, receiver antenna gain, longitude and latitude of specular point
GloWS-Net	BRCS DDM, effective scattering area	NBRCS, LES, TES, SNR, incidence angle, receiver antenna gain, longitude and latitude of specular point, swell SWH, wave direction, rainfall intensity

Determining the optimal activation function in neural networks is an important task because it is directly related to network performance. Unfortunately, however, it is difficult to determine this function analytically. On the contrary, an optimal activation function is usually determined through repeated trials or adjustments [63]. This paper considers five activation functions, namely Relu, Tanh, Elu, Sigmoid and softplus:

$$f_{\text{Relu}}(x) = \max(0, x) = \begin{cases} 0, & x < 0 \\ x, & x >= 0 \end{cases} \tag{1}$$

$$f_{\text{Tanh}}(x) = \frac{2}{1 + e^{-2x}} - 1 \tag{2}$$

$$f_{\text{Elu}}(x) = \begin{cases} x, & x > 0 \\ \alpha(\mathrm{e}^{x} - 1), & x \leqslant 0 \end{cases} \tag{3}$$

$$f_{\text{Sigmoid}}(x) = \frac{1}{1 + e^{-x}} \tag{4}$$

$$f_{\text{Softplus}}(x) = \ln(1 + \exp(x)) \tag{5}$$

In the above formula, x is the input value of the previous layer neuron.

The advantage of the Sigmoid activation function is that the gradient is smooth, avoiding jumping output values. However, the gradient tends to be zero, so the exponential calculation is slow. The Tanh function has some advantages over the Sigmoid function. However, when the input is large or small, the output is almost smooth and the gradient is small, which is not conducive to weight update. The Relu function is a popular activation function in deep learning. Compared with the Sigmoid function and Tanh function, the Relu function does not have the gradient saturation problem, and because the Relu function only has a linear operation function, its calculation speed is faster than the Sigmoid function and Tanh function. However, the Relu function also has disadvantages. For example, when the input is negative, in the back propagation process, the gradient will be completely zero.The Elu function solves the problem of Relu. Compared with Relu, Elu has a negative value, which will make the average value of activation close to zero. The mean activation close to zero can make learning faster because it makes the gradient closer to the natural gradient. Please note that although the Elu function is better than the Relu function in theory, there is no sufficient evidence to show that Elu is always better than Relu in practice. The Softplus function is similar to the Relu function, but it is relatively smooth. As with Relu, it has unilateral suppression and has a wide acceptance range (i.e., (0, +inf)).

In order to determine the activation function for optimal performance, we analyzed and discussed the influence of the number of neurons in different hidden layers and different activation functions on the accuracy of wind speed retrieval using the FCN architecture. Generally, the accuracy of linear models is low, so the activation function improves the performance of the FCN model by adding nonlinear factors. As stated in [38], the number of hidden layers used in FCN is usually between 1 and 3, and 4 layers are rarely used because more hidden layers will cause a higher computing cost [38]. Generally, the FCN architecture with three hidden layers can obtain the best results in wind speed retrieval [50]. Therefore, we also adopted the FCN architecture with three hidden layers, and set the number

of neurons in each layer to 4N, 2N and N, respectively, with N being 4, 8, 12, 24, 32, 48, 64 or 128.

Figure 4 shows the RMSE comparison of wind speed retrieval performance for the different number of neurons and different activation functions in the three hidden layers. It can be seen from the figure that different activation functions have a great impact on the accuracy of wind speed retrieval, so it is very important to select an appropriate activation function. When N = 128, the Relu activation function achieves the best performance in RMSE, followed by the Tanh function. Therefore, this paper uses the Relu function as the best activation function for all neural network architectures, and the hidden layers of FCN1, FCN2, FCN3 and FCN4 models are set as 512, 256 and 128, respectively.

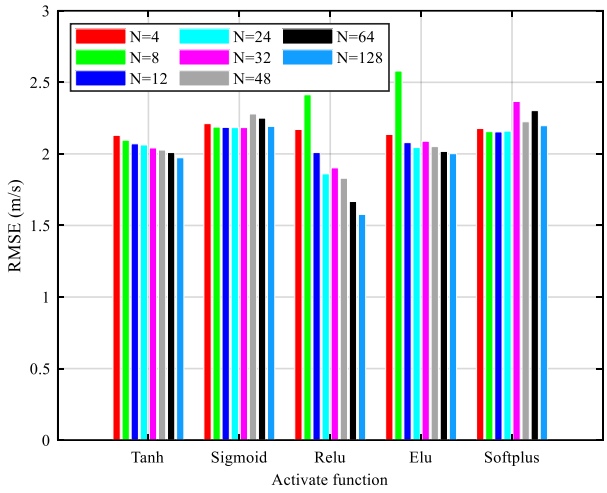

Figure 4. Comparison of different activation functions.

In this paper, the mean square error between the predicted wind speed and the reference wind speed is used as a loss function:

$$\text{Loss} = \frac{1}{N}\sum_{i=1}^{N}(\hat{u}_i - u_i)^2 \tag{6}$$

where N is the number of samples, $\hat{u}_i$ is the predicted wind speed, and u_i is the reference wind speed.

The optimizer is another important configuration of the training model. After comparison, we chose Adam optimization algorithm to train small batches randomly disordered.

3.3. GloWS-Net Model Training and Verification

The related network is implemented under the Keras architecture and TensorFlow backend. Table 4 shows the basic configuration of the experimental platform. These networks can be trained on the GeForce GTX 1050Ti GPU. The preprocessed data are normalized to zero mean and unit variance according to the characteristics. The verification set is used to avoid overfitting. We adopt the early stop condition with six epochs. The learning rate is set to 0.0005. To further prevent the overfitting problem, the random deactivation (dropout) is set to 0.1.

The training set and verification set are separated. The training set is used to train the network model, and the verification set is used to supervise the model training. The batch size in this paper is set to 32. When the network updates the weight coefficient each time, only samples from one batch are used to train the model. To ensure good performance, the number of epoch is set to 100.

Table 4. The configuration of experiment platform.

Programming Language	Python 3.7
Deep learning API	Tensorflow 2.3 and Keras 2.4
CPU	Intel core i7-7700HQ
Running memory	16 GB
GPU	GeForce GTX 1050Ti

4. Performance Analysis and Discussion of Wind Speed Retrieval

4.1. Comparison with ERA5 Data

In this section, the performance of the GloWS-Net model architecture is compared with the traditional MVE method and some existing network architectures (such as FCN and CNN models). The wind speed retrieval performance test is conducted on the test data set, which is not used during training and is separated from the training set and verification set. Therefore, it is very suitable for evaluating the generalization ability of corresponding network models on blind data sets. However, this training method also has a disadvantage that any systematic errors will be invisible to the algorithm. In the following, we first compare and analyze the wind speed retrieval performance of different retrieval models, then evaluate the performance of different retrieval models in retrieving global wind speed, and finally discuss the results.

As shown in Figure 1 above, wind speed retrieval can be divided into two stages. The first stage involves the GMF method, CNN1, CNN2, FCN1, FCN2, FCN3 and FCN4 models. The second stage includes wind speed retrieval by CNN3 model and GloWS-Net model. Among them, the CNN3 model fuses the DDM image and auxiliary parameters excluding SWH, wave direction and rainfall information. The GloWS-Net model includes SWH of swell, wave direction and rainfall information as input parameters. Table 5 shows the retrieval accuracy statistics of different retrieval models for wind speed less than 10 m/s, 10–15 m/s, 15 m/s and 0–30 m/s. In the table, RMSE, mean absolute error (MAE), correlation coefficient (CC) and MAPE represent root mean square error, mean absolute error, correlation coefficient and mean absolute percentage error, respectively. The following conclusions can be drawn from the table:

Table 5. Accuracy of wind speed retrieved from different models using ERA5 data as reference.

Models	<10 m/s	10–15 m/s	>15 m/s	0–30 m/s			
	RMSE (m/s)	RMSE (m/s)	RMSE (m/s)	RMSE (m/s)	MAE (m/s)	CC	MAPE (%)
NBRCS	2.05	2.46	4.48	2.42	1.85	0.83	29.93
LES	2.26	2.54	4.65	2.71	1.98	0.70	32.41
MVE	2.23	2.42	4.29	2.53	1.98	0.81	30.64
FCN1	2.48	2.52	4.08	2.66	2.08	0.80	31.69
FCN2	1.78	2.02	3.33	2.03	1.57	0.89	23.40
FCN3	1.61	2.13	3.42	1.99	1.52	0.89	22.63
FCN4	1.76	1.89	2.89	1.92	1.48	0.90	24.78
CNN1	1.71	2.59	4.68	2.37	1.81	0.85	25.72
CNN2	2.05	2.46	4.54	2.46	1.90	0.82	28.64
CNN3	1.81	2.18	2.81	2.02	1.53	0.89	21.91
GloWS-Net	1.69	2.10	2.68	1.92	1.43	0.90	20.67

(1) When the wind speed is within the range of 0-30 m/s, the RMSE of the FCN4 and the proposed GloWS-Net model architectures are the lowest (1.92 m/s). However, it can be observed from the table that the proposed GloWS-Net model architecture is superior to the FCN4 model in terms of MAE and MAPE, especially for MAPE. Generally, MAE and MAPE are less affected by extreme values. However, RMSE uses the square of error and it is more sensitive to outliers. The FCN3 and CNN3 model architectures with the

same number of auxiliary parameter inputs also show a similar situation, which indicates that after adding DDM images, the GloWS-Net model architecture can obtain the same RMSE as the FCN model, but MAPE has been significantly improved by 16.56%. In addition, in terms of the four indicators (MRSE, MAE, CC and MAPE), the performance of the proposed GloWS-Net model architecture is significantly better than the model combing the results from NBRCS and LES based on the MVE method, with an increase of 23.98%, 27.95%, 11.02% and 32.52%, respectively. Compared with the NBRCS method, it increased by 20.67%, 22.78%, 8.95% and 30.92%, respectively. Compared with the LES method, it has increased by 29.16%, 27.85%, 29.19% and 36.21%, respectively.

(2) In the case of strong wind (>15 m/s), the RMSE of all architectures and MVE methods increases. However, adding auxiliary parameters, as done in FCN2, FCN3, FCN4, CNN3, and GloWS-Net model architectures, will reduce RMSE. Compared with other architectures, CNN1 and CNN2 that only handle BRCS DDM or power DDM have poor performance. This shows that even when the wind speed is lower than 9 m/s, it is necessary to add auxiliary parameters to obtain satisfactory results. It is encouraging to note that the GloWS-Net model architecture has the best performance in retrieving wind speed under strong wind conditions and has obtained the minimum RMSE.

(3) In the case of moderate wind speed (10–15 m/s), the retrieval performance of FCN4 and GloWS-Net model architecture is better than that of the GMF method. However, the performance of GloWS-Net is slightly inferior to that of FCN4. Under low wind speed (<10 m/s), the performance of GloWS-Net is slightly better than that of FCN4. In this case, although the RMSE of the MVE method is small, it is still worse than FCN (such as FCN2, FCN3 and FCN4), CNN (CNN1, CNN2 and CNN3) and GloWS-Net. In addition, it is worth noting that the accuracy of the FCN1 model with only NBRCS and LES observables as auxiliary parameters is much lower than that of the traditional MVE method, which indicates that more auxiliary parameters need to be added to the FCN1 model for wind speed retrieval to obtain satisfactory results (such as FCN2, FCN3 and FCN4). Another important aspect we can notice is that the CNN1 model with BRCS DDM as the input only achieves the same performance as the FCN4 and GloWS-Net model architectures under low wind speed. This shows that the CNN1 wind model for low wind speed can benefit from the accretion layer.

In sum, in terms of overall RMSE, except for FCN1, CNN1 and CNN2, other model architectures have better wind speed retrieval performance than the NBECS, LES and MVE methods. For the accuracy obtained from the wind speed range of 0–30 m/s, although the RMSEs of GloWS-Net and FCN4 are equivalent, the performance of the proposed GloWS-Net is better than that of FCN4 in terms of MAE and MAPE, especially for MAPE. In addition, FCN4 performs worse than GloWS-Net under low and high wind speeds. It should be emphasized that only a verification using in situ measurements provided by weather stations or a campaign with boats on the investigated area will fully validate the proposed approach.

In order to evaluate the performance of different models, Figure 5 shows the wind speed scatter density plots of different models and ERA5. The color bar in the figure represents the data density, the red dotted line represents the 1:1 reference line, the magenta solid line represents the linear fitting result between the retrieved and ERA5 wind speeds, and the CC represents Pearson correlations between retrieved wind speed of the model and ERA5 wind speed are also given. The following observations can be seen from the figure:

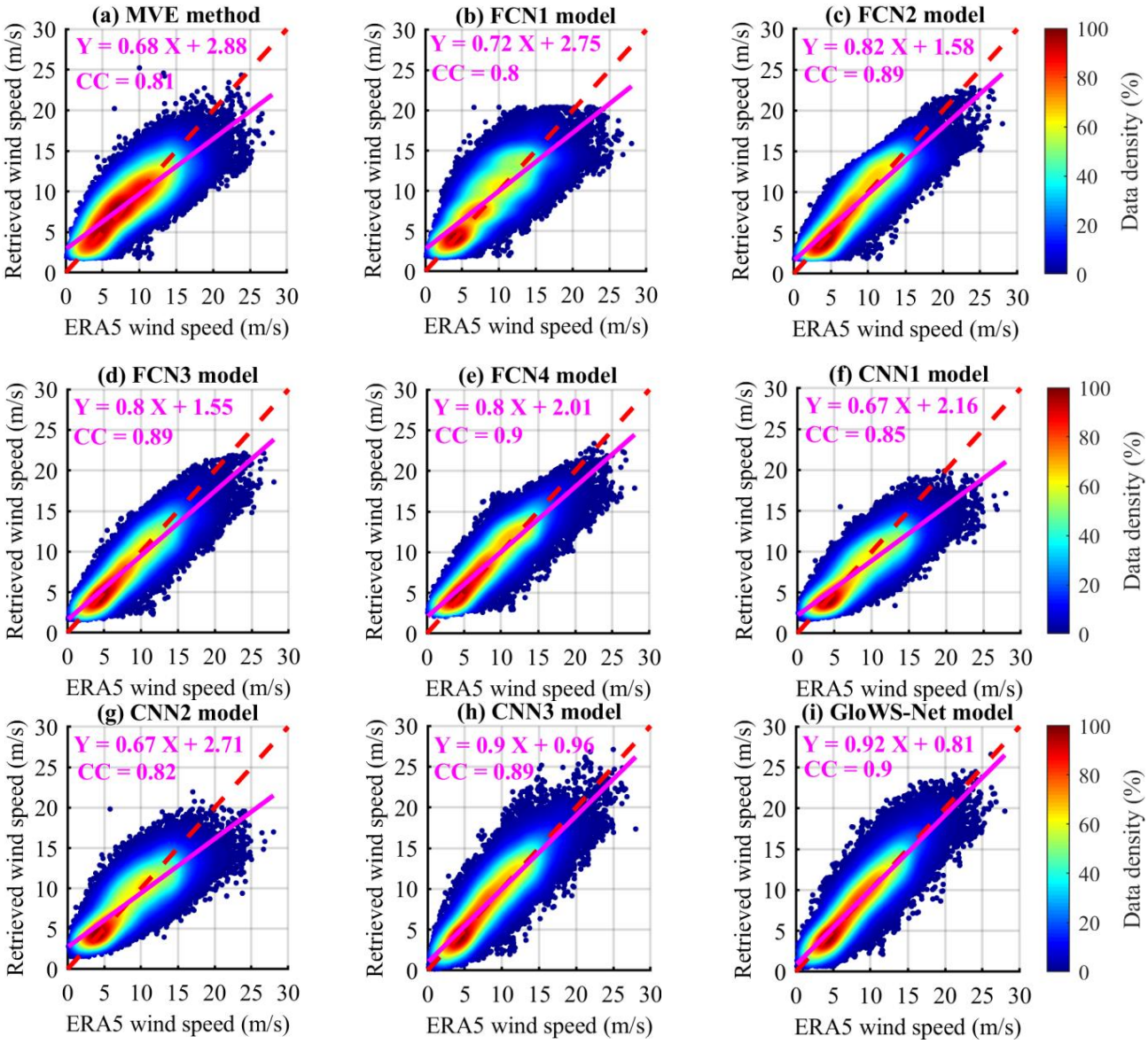

Figure 5. Scatter density plots of retrieved wind speed by different models and ERA5 wind speed.

(1) Although the FCN4 model analyzed above and the GloWS-Net model produce the same RMSE, the proposed GloWS-Net model and CNN3 model show better performance in terms of correlation between retrieved wind speed and ERA5 data. Obviously, there are more data points distributed symmetrically along the y = x line, and fewer data points scattered around the line.

(2) The MVE method obviously overestimated the wind speed of 5 to 12 m/s, which may be caused by insufficient power calibration of CYGNSS data and high noise [48,54]. Within this range, a large number of samples and some measured power values may be underestimated. This problem has been improved by FCN, CNN and GloWS-Net. In particular, the results retrieved by CNN3 and GloWS-Net both are more concentrated along the 1:1 reference line when wind speed is in the range of 5~12 m/s. It is also obvious from the figure that the MVE method, FCN1, FCN2, FCN3, FCN4, CNN1 and CNN2 model architectures have poor response capability to wind speed in the range of 0–5 m/s. However, CNN3 and GloWS-Net model architectures do not have this problem. This shows that after adding DDM images to the input layer of the CNN3 and GloWS-Net wind models, the architecture incorporating the convolution layer has better performance than those with only the full connection layer because they use the patterns in DDM. In addition, except

for CNN3 and GloWS-Net, other models show overestimation at very low wind speeds (<5 m/s) and underestimation at high wind speeds (15–30 m/s). The correlation between the wind speed retrieved by CNN1 and CNN2 models and the ERA5 data is the worst, which clearly indicates that more auxiliary parameters need to be included in CNN1 and CNN2 to obtain better results.

(3) It is worth mentioning that, compared with the two most advanced deep learning model architectures (i.e., MCNN and CyGNSSnet) currently used for spaceborne GNSS-R wind speed retrieval [40,41], the GloWS-Net model architecture proposed in this paper performs very well in the case of high wind speed, that is, the GloWS-Net model significantly mitigates the underestimation phenomenon at high wind speed. Generally, for marine disasters caused by marine events with large wind speeds such as hurricanes and typhoons, high-precision wind speed estimation results at high wind speeds are very helpful for monitoring those disasters. Although limited to the current level of spaceborne GNSS-R technology, wind speed prediction under strong winds is still facing great challenges [64,65]. However, the excellent performance of the GloWS-Net model at high wind speeds is promising for future marine disaster monitoring.

Figure 6 shows the RMSE and MAE of different models for different wind speed ranges. It can be seen that CNN3 and GloWS-Net outperform other architectures especially for challenging high wind speeds (>20 m/s). In addition, when the wind speed is greater than 8 m/s, it can be seen that including SWH, wave direction and rainfall information enhances the model performance. However, when the wind speed is greater than 20 m/s, the CNN3 model shows equivalent performance as the GloWS-Net model architecture. The reason may be that strong wind speed is accompanied by heavy rainfall or strong wind speed causes dramatic changes in sea conditions. Even if rainfall, swell and wave direction information is introduced into the GloWS-Net model framework, it is difficult to correct these influencing factors completely. Therefore, future research needs to further optimize the GloWS-Net model architecture.

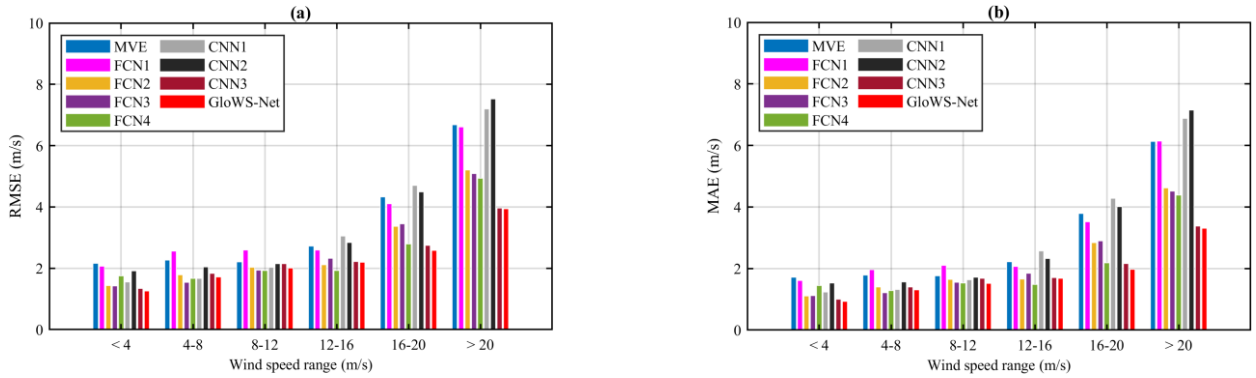

Figure 6. When ERA5 wind speed is used as reference for (**a**) RMSE and (**b**) MAE for different wind speed ranges.

In order to compare the global performance of wind speed retrieved by GloWS-Net and the traditional model, we selected the period from July to August 2021 in the test data set for analysis. Figure 7 shows the ERA5 wind speed and the results retrieved using the MVE method, FCN4 and GloWS-Net. Figure 8 shows the deviation distribution histogram between ERA5 wind speed and the results obtained by the MVE method, FCN4 as well as GloWS-Net. In the figure, the average deviation (μ), standard deviation (σ), mean absolute error (MAE) and 80% quantile (Qua) of the deviation are also given. The blue bar chart depicts the error distribution, the red dotted line represents the fitting curve of the probability density function of the error and the green dotted line marks the wind speed deviation of 0 m/s. It can be observed from Figure 7 that the performance of FCN4 and GloWS-Net is better than the MVE method in retrieving global wind speed, and the results from the MVE method are significantly different from the ERA5 data in multiple sea areas around

the world (as shown by the magenta rectangle mark in the figure). Comparing the wind speed retrieval results of FCN4 and GloWS-Net with the ERA5 data, it is found that the performance of the GloWS-Net model is better. For example, in the sea area within the longitude of 60°E–120°E and the latitude of 10°S–40°S, the FCN4 model shows an underestimated wind speed, while the retrieved wind speed of the GloWS-Net model is highly consistent with the ERA5 data. From Figure 8, it can also be seen that the performance of the GloWS-Net model is better than that of the FCN4 model. The deviation between the GloWS-Net model wind speed results and the ERA5 data is very concentrated (80% of the wind speed deviation is less than 2.28 m/s) and near the deviation line of 0 m/s, while the wind speed deviation of FCN4 is on the left side of the green line in the histogram. The negative deviation is more obvious, and 80% of the wind speed deviation is less than 2.34 m/s. From the wind speed deviation histograms of the three models, the global wind speed retrieved by the MVE method is the worst, and 80% of the wind speed deviation is 3.20 m/s. The above analysis further confirms that the GloWS-Net model architecture has strong advantages in retrieving global sea surface wind speed.

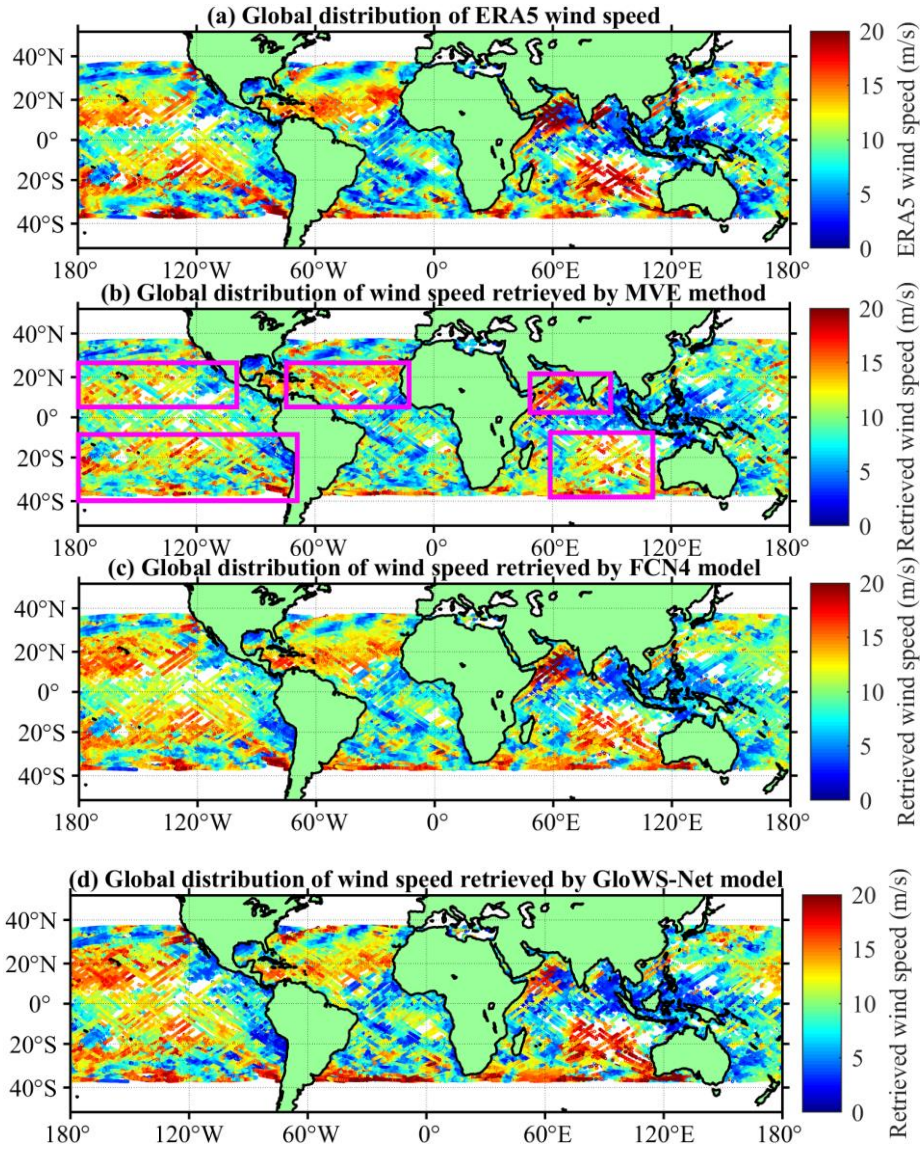

Figure 7. Global distribution of ERA5 wind speed data and retrieved wind speed by different models.

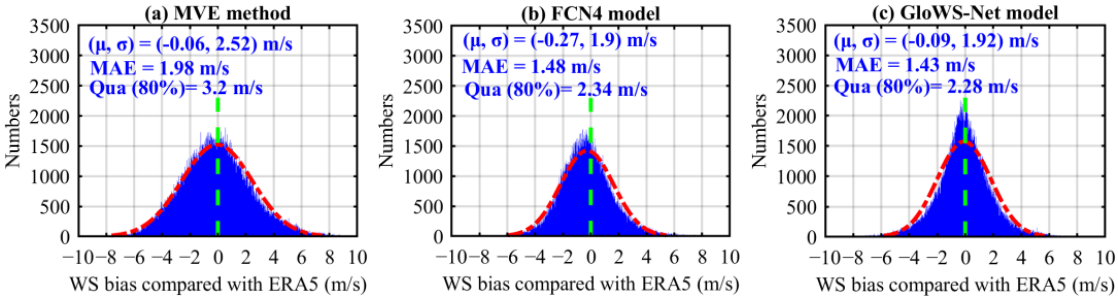

Figure 8. Deviation distribution histograms between ERA5 wind speed and retrieved wind speed by different models.

4.2. Comparison with CCMP Data

It is necessary to evaluate the wind speed retrieval performance of the proposed deep model through independent wind speed measurement. The CCMP wind speed is closer to conventional in situ measurements from ships than the ERA5 product. In [66], CCMP winds and Tropical Atmosphere Ocean (TAO) mooring observations were compared; a good agreement with a root mean square error (RMSE) of 1 m/s and a correlation coefficient of 0.95 were obtained. The CCMP wind product is a newly released global ocean wind data set and suitable for scientific study at various temporal and spatial resolutions, which is widely used to verify the retrieval of wind speed by spaceborne GNSS-R [55,67,68]. Therefore, the wind speed of CCMP was also collected and compared with the retrieved wind speed. Figure 9 shows the correlation between the ERA5 wind speed data and CCMP wind speed data used in the test model in this study, as well as the probability density function (PDF) distribution curve of ERA5 and CCMP wind speeds. These data cover a wind speed range of 0 to 30 m/s, but only a few samples have wind speeds of 20–30 m/s, which may lead to low accuracy at high wind speeds. We can see that the PDF of the two data sets is almost the same, except that ERA5 wind speed is slightly higher than CCMP at 3–6 m/s and vice versa at 14–19 m/s. This may be due to the differences in the platforms, hardware and algorithms used to generate the two data sets. In addition, the RMSE and CC between the two data sets are 1.46 m and 0.95, respectively, which are highly correlated.

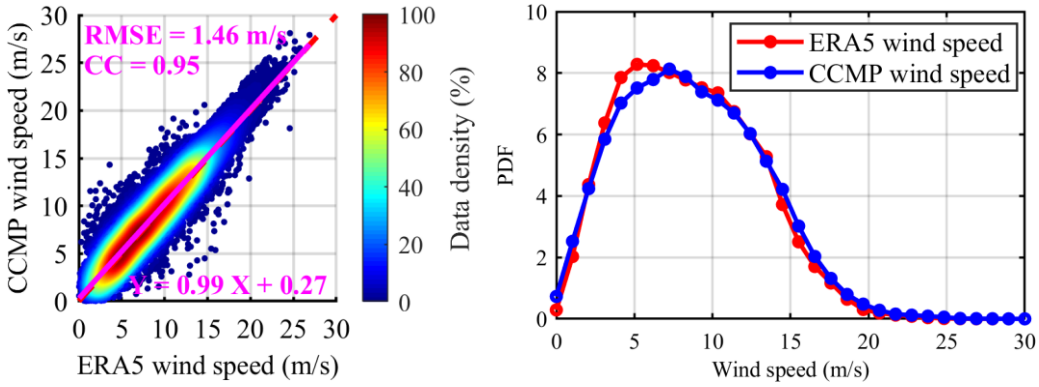

Figure 9. Scatter density plots of ERA5 and CCMP wind speed (**left**) and probability density function (PDF) distribution using ERA5 (the red line) and CCMP (the blue line) products as reference in the testing set (**right**).

Table 6 shows the accuracy statistics by comparing the retrieved wind speed data of different models with the CCMP data. The following conclusions can be drawn from the table:

Table 6. Accuracy of wind speed retrieved from different models using CCMP data as reference.

Models	<10 m/s	10–15 m/s	>15 m/s	0–30 m/s			
	RMSE (m/s)	RMSE (m/s)	RMSE (m/s)	RMSE (m/s)	MAE (m/s)	CC	MAPE (%)
NBRCS	2.23	2.58	4.53	2.61	2.06	0.81	30.89
LES	2.45	2.63	4.78	2.87	2.15	0.68	42.36
MVE	2.47	2.52	4.47	2.71	2.12	0.79	41.84
FCN1	2.71	2.63	4.33	2.86	2.22	0.78	42.87
FCN2	1.98	2.18	3.59	2.22	1.71	0.87	31.69
FCN3	1.80	2.27	3.68	2.16	1.66	0.87	31.45
FCN4	2.00	2.07	3.16	2.14	1.67	0.88	36.11
CNN1	1.91	2.66	4.76	2.49	1.92	0.84	33.80
CNN2	2.26	2.52	4.62	2.60	2.02	0.80	37.60
CNN3	2.05	2.33	2.97	2.23	1.70	0.87	29.79
GloWS-Net	1.97	2.34	2.80	2.16	1.65	0.88	29.70

(1) When the wind speed is within the range of 0–30 m/s, the RMSE of the FCN4 model architecture is the lowest (2.14 m/s), followed by the proposed GloWS-Net model architecture (RMSE = 2.16 m/s) and FCN3 model architecture. The results of comparison between retrieved wind speed and CCMP are similar to those of ERA5, the difference of RMSE between the GloWS-Net model architecture and FCN model is very small, but MAPE has been significantly improved by 17.75%. Moreover, in terms of the four indicators (MRSE, MAE, CC and MAPE), the performance of the proposed GloWS-Net model architecture is much better than the model combining the results from NBRCS and LES based on the MVE method, with an increase of 20.27%, 22.21%, 11.20% and 29.02%, respectively. Compared with the NBRCS method, it is increased by 17.20%, 20.11%, 8.89% and 3.86%, respectively. Compared with the LES method, it is increased by 24.71%, 23.45%, 29.70% and 29.90%, respectively.

(2) In the case of strong wind (>15 m/s), except for the GloWS-Net model architecture, the RMSE of wind speed retrieved from other models is large. The RMSE of the GloWS-Net model is 2.8 m/s, and the retrieval accuracy is 37.42% and 11.58% higher than that of the MVE and FCN4 models, respectively.

(3) Under medium (10–15 m/s) and low (<10 m/s) wind speed, the results of the comparison between retrieved wind speed and CCMP are similar to those of ERA5. Among them, the GloWS-Net and FCN4 model retrieved wind speed has good correlation with the CCMP data.

Figure 10 shows the wind speed scatter density plots of different models and CCMP. It can be seen that the comparison results between the wind speed retrieved by different models and CCMP are consistent with those with the ERA5 data. This further shows that the GloWS-Net model proposed in this paper is reliable and has high generalization ability, which means it is good for practical application.

It is also necessary to evaluate the retrieval performance of different retrieval models in different wind speed ranges when the CCMP wind speed data are used as reference. Figure 11 shows the RMSE and MAE for different wind speed ranges. It can be seen that CNN3 and GloWS-Net outperform other architectures especially for challenging high wind speeds (> 20 m/s). Furthermore, when the wind speed is greater than 8 m/s, it can be seen that including SWH, wave direction and rainfall information also improves the GloWS-Net model performance. When the wind speed is greater than 20 m/s, the GloWS-Net model shows the best retrieval performance.

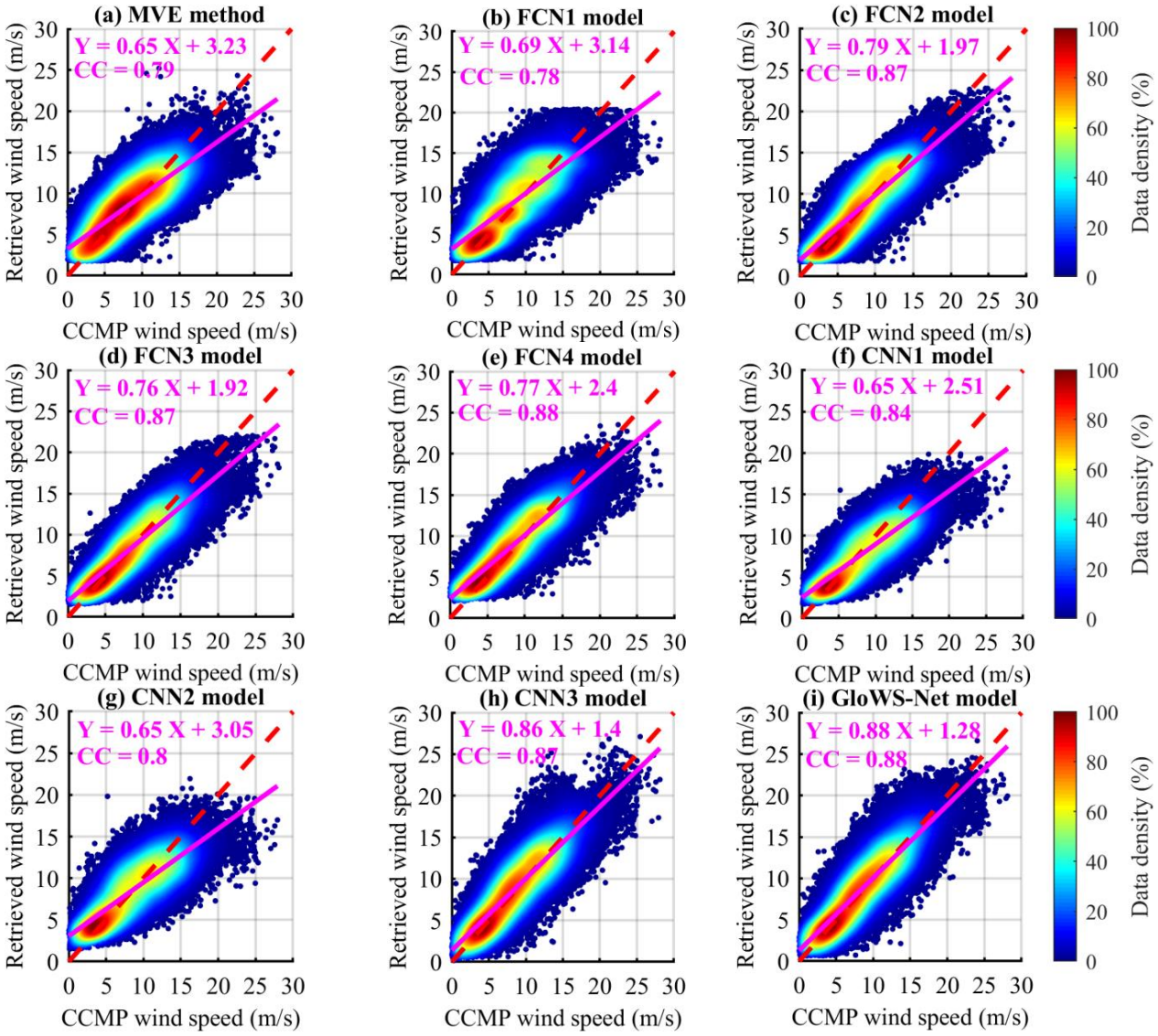

Figure 10. Scatter density plots of retrieved wind speed by different models and CCMP wind speed.

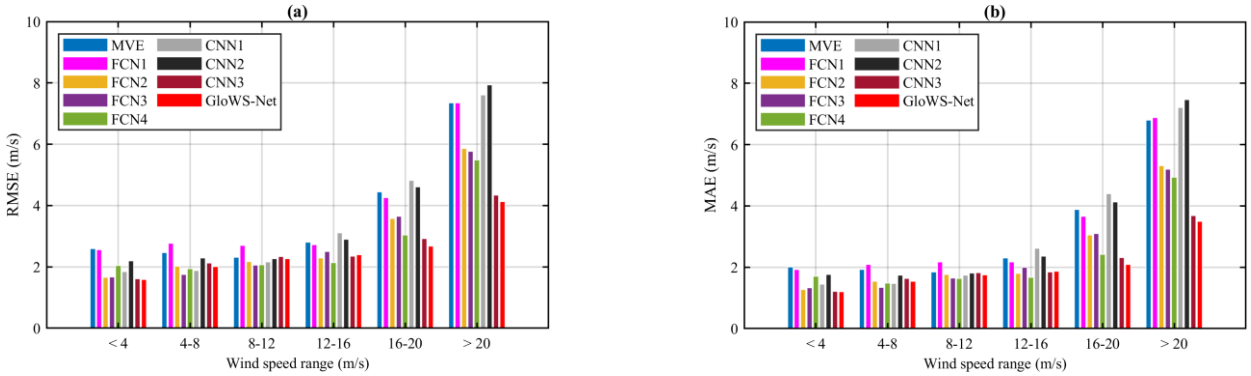

Figure 11. (**a**) RMSE and (**b**) MAE for different wind speed ranges when CCMP wind speed is used as reference.

Figure 12 shows the global deviation distribution histogram between CCMP wind speed and the results obtained by the MVE method and FCN4 as well as GloWS-Net. From Figure 12, it can also be seen that the performance of the GloWS-Net model is better than

that of the FCN4 model. The deviation between the GloWS-Net model wind speed results and the ERA5 data is very concentrated (80% of the wind speed deviation is less than 2.60 m/s) and near the deviation line of 0 m/s, while 80% of the wind speed deviation of FCN4 model is less than 2.62 m/s, the global wind speed retrieved by the MVE method is the worst, and 80% of the wind speed deviation is 3.39 m/s. The above analysis further proves that the GloWS-Net model architecture has the best generalization ability in retrieving global sea surface wind speed.

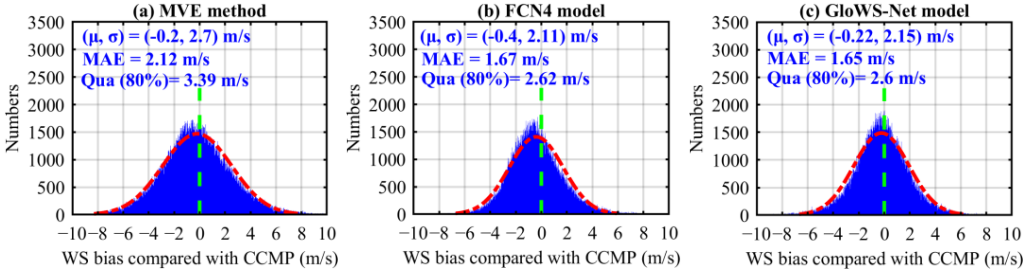

Figure 12. Deviation distribution histograms between CCMP wind speed and retrieved wind speed by different models.

4.3. Discussion

Previous research has successfully utilized a fully connected network (FCN) model for wind speed retrieval [37–43]. Inspired by image processing technology, Asgarimehr and Guo et al. studied spaceborne GNSS-R wind speed retrieval based on deep learning methods (CyGNSSnet and MCNN) [40,41]. Although both models employ the features extracted from BRCS DDM, MCNN also uses effective scattering area as the input image. However, their research shows that the GNSS-R wind speed retrieval model can benefit from the convolution layer. Because the image information in the DDM is integrated, the architecture that combines the convolution layer and the full connection layer has better performance than the architecture that only has the full connection layer. However, the retrieval results of both their models and the GloWS-Net model architecture proposed in this paper show that, mainly in the case of high wind speed, the model architecture integrating layer that takes DDM as input with the fully connection layer that takes auxiliary parameters as input can obtain more obvious accuracy improvement than the FCN model, but their RMSE improvement in the whole wind speed range of 0–30 m/s is not significant. This may require further optimization of the convolutional layer architecture or training of special models for different wind speed ranges [50]. However, the GloWS-Net model architecture proposed in this paper is superior to the FCN model architecture in MAE and MAPE, especially in MAPE. From this point of view, GloWS-Net achieves better performance improvement than CyGNSSnet and MCNN for the wind speed range of 0–30 m/s.

Although CNN extracts features directly from the input, research shows that the prediction accuracy of CNN can be improved by using traditional features. For example, the combination of CNN and handmade features enhances image classification [69,70]. Similarly, theoretical remote sensing knowledge is increasingly combined with deep learning to further improve its performance [71]. The analysis in this paper also shows that traditional CNN models (such as CNN1 and CNN2) without full connection layer to combine auxiliary parameters and DDM result in an RMSE of 2.46 m/s. The performance of fully connected architectures (such as FCN1) with NBRCS and LES as input characteristics is inferior to CNN1 and CNN2, resulting in an RMSE of 2.66 m/s. However, under high wind speed (>15 m/s), the performance of FCN1 is better than that of CNN1 and CNN2. Therefore, the use of convolution layers to directly extract features from DDM, combined with more auxiliary feature parameters including NBRCS and LES, can provide the best performance (such as CNN3 and GloWS-Net models), and RMSE is better than 1.92 m/s. By comparing the performance of FCN4 and GloWS-Net, it can be concluded that adding more auxiliary parameters does not necessarily reduce the RMSE of the test data. Although

previous research and the results in this paper show that these auxiliary parameters can improve the retrieval performance of the model, and based on this fact, they have been selected as the input of the full connection layer. Therefore, it is necessary to further optimize the previously proposed model and GloWS-Net model architecture.

MVE is a classical method for retrieving sea surface wind speed. According to the statistical results in Tables 5 and 6, the GloWS-Net model framework is superior to the MVE method in all wind speed ranges. Especially at high wind speeds (>15 m/s), RMSE is decreased by 37.45%, which shows significant improvement compared with previous studies. Figures 8 and 12 also confirm that the global performance of the GloWS-Net model framework is better than MVE and FCN4, and the deviation has improved globally. Compared with the recent model based on the full connection layer for processing CYGNSS data [36,38], the GloWS-Net model architecture also shows encouraging performance. However, the differences in data length, version, quality control, filtering and validation methods should be considered to ensure the estimation of new data sets will have the same accuracy.

Both MVE and GloWS-Net underestimated high wind speed, which may be caused by the sensitivity saturation of DDM observed under strong wind conditions [32]. This is a common problem of radar scatterometer whose performance will be reduced under high wind speed [72]. However, compared with previous CyGNSSnet and MCNN models, the GloWS-Net model has significantly improved the wind speed retrieval performance in the case of large wind speed, showing good consistence with the ERA5 data. However, it is still challenging to use the GloWS-Net model to retrieve high wind speed. Due to the relatively small number of high wind speed samples involved in the training model, the performance of the deep learning algorithm is limited when the wind speed is greater than 15 m/s.

Figure 7 shows the area with overestimated wind speeds, especially in the Asia Pacific region with longitude between 50°W–0°. This is consistent with the situation reported by Asgarimehr et al. [40]. This area is strongly affected by the L-band signal of the Quasi Zenith Satellite System (QZSS), which may be a potential source of Radio Frequency Interference (RFI). RFI caused by other L-band signals, especially satellite enhancement system (SBAS) signals, has been considered as the root cause of the reduction of signal to noise ratio and the wind speed overestimation of GNSS-R [73]. Asgarimehr et al. also reported similar overestimation in the equatorial region in TDS-1 satellite measurements [74]. Please note that the similarity of wind speed retrieved by MVE, CyGNSSnet and GloWS-Net confirms that overestimation is related to the data quality but not due to the retrieval methods.

5. Conclusions

This paper studies the method of retrieving sea surface wind speed using spaceborne GNSS-R data from CYGNSS mission observations, and proposes a GloWS-Net deep learning network model architecture for spaceborne GNSS-R global sea surface wind speed retrieval. Extensive test results show that the GloWS-Net model architecture can obtain the same retrieval accuracy as the FCN model with respect to RMSE, but MAPE has been significantly improved. When compared with ERA5 wind speed and CCMP wind speed, the MAPE improved by 16.56% and 17.75%, respectively. Moreover, when using ERA5 winds as ground truth, compared with the MVE method, RMSE, MAE, CC and MAPE are improved by 23.98%, 27.95%, 11.02% and 32.52%, respectively, when using CCMP winds as ground truth, RMSE, MAE, CC and MAPE are improved by 20.27%, 22.21%, 11.20% and 29.02%, respectively. Compared with previous FCN, CNN, CyGNSSnet and MCNN models, the proposed wind speed retrieval method based on the GloWS-Net model has achieved promising overall performance. The research results also show that the GloWS-Net model architecture has strong advantages in retrieving global sea surface wind speed. In particular, the GloWS-Net model significantly reduces the underestimate phenomenon at high wind speeds. Compared with CyGNSSnet and MCNN, it also performs very well. Being limited by current spaceborne GNSS-R technology level, it still faces a huge chal-

lenge to precisely predict wind speed under strong winds. However, the excellent performance of the GloWS-Net model at high wind speeds is promising for future marine disaster monitoring. As we know, buoy data have been widely used as ground truth for validation. Due to limited access and spatial coverage of the buoy (NDBC, TAO, etc.) data, the ERA5 and CCMP data have been employed as the comparison data in this study. In the future, further validation using buoy data can be conducted once such high quality data are available.

Author Contributions: All authors have made significant contributions to this manuscript. J.B. partly designed the improved method, analyzed the data, wrote the initial version of paper and validated the improved method; K.Y., X.Z. and W.H. conceived the improved method, wrote the revised version of the paper and provided supervision; J.B., K.Y., X.Z., J.N., Y.L. and W.H. checked and revised this paper. All authors have read and agreed to the published version of the manuscript.

Funding: This work was supported in part by the National Natural Science Foundation of China under Grants 42161067 and 42174022, in part by the major scientific and technological projects of Yunnan Province: Research on Key Technologies of ecological environment monitoring and intelligent management of natural resources in Yunnan under Grant 202202AD080010, in part by the Postgraduate Research and Practice Innovation Program of Jiangsu Province under Grant KYCX20_2003, in part by the Future Scientists Program of China University of Mining and Technology under Grant 2020WLKXJ049, in part by the China Scholarship Council (CSC) through a State Scholarship Fund (No.202106420009), and in part by the Programme of Introducing Talents of Discipline to Universities, Plan 111, Grant No. B20046.

Data Availability Statement: Not applicable.

Acknowledgments: We would like to thank NASA for providing the CYGNSS data, the European Center for Medium-Range Weather Forecasts (ECMWF) for providing wind speed, wave direction and swell height data, the NASA for providing GPM-IMERG rainfall data, and the developers of Cross-Calibrated Multi-Platform (CCMP) wind product for providing the data freely available to the public. The authors also thank the anonymous reviewers for their in-depth reviews and helpful suggestions that have largely contributed to improving this paper.

Conflicts of Interest: The authors declare no conflict of interest.

References

1. Li, C.; Huang, W.; Gleason, S. Dual Antenna Space-Based GNSS-R Ocean Surface Mapping: Oil Slick and Tropical Cyclone Sensing. *IEEE J. Sel. Top. Appl. Earth Observ. Remote Sens.* **2015**, *8*, 425–435. [CrossRef]
2. Mayers, D.; Ruf, C. Tropical cyclone center fix using CYGNSS winds. *J. Appl. Meteorol. Climatol.* **2019**, *58*, 1993–2003. [CrossRef]
3. Wang, S.; Shi, S.; Ni, B. Joint Use of Spaceborne Microwave Sensor Data and CYGNSS Data to Observe Tropical Cyclones. *Remote Sens.* **2020**, *12*, 3124. [CrossRef]
4. Foti, G.; Gommenginger, C.; Srokosz, M. First Spaceborne GNSS-Reflectometry Observations of Hurricanes from the UK TechDemoSat-1 Mission. *Geophys. Res. Lett.* **2017**, *44*, 12358–12366. [CrossRef]
5. Ruf, C.; Atlas, R.; Chang, P.; Clarizia, M.P.; Garrison, J.; Gleason, S.; Katzberg, S.; Jelenak, Z.; Johnson, J.; Majumdar, S.; et al. New Ocean Winds Satellite Mission to Probe Hurricanes and Tropical Convection. *Bull. Am. Meteorol. Soc.* **2016**, *97*, 385–395. [CrossRef]
6. Jing, C.; Niu, X.; Duan, C.; Lu, F.; Di, G.; Yang, X. Sea Surface Wind Speed Retrieval from the First Chinese GNSS-R Mission: Technique and Preliminary Results. *Remote Sens.* **2019**, *11*, 3013. [CrossRef]
7. Yang, G.; Bai, W.; Wang, J.; Hu, X.; Zhang, P.; Sun, Y.; Xu, N.; Zhai, X.; Xiao, X.; Xia, J.; et al. FY3E GNOS II GNSS Reflectometry: Mission Review and First Results. *Remote Sens.* **2022**, *14*, 988. [CrossRef]
8. Clarizia, M.P.; Ruf, C.; Cipollini, P.; Zuffada, C. First spaceborne observation of sea surface height using GPS-Reflectometry. *Geophys. Res. Lett.* **2016**, *43*, 767–774. [CrossRef]
9. Li, W.; Rius, A.; Fabra, F.; Cardellach, E.; Ribo, S.; Martin-Neira, M. Revisiting the GNSS-R Waveform Statistics and Its Impact on Altimetric Retrievals. *IEEE Trans. Geosci. Remote Sens.* **2018**, *56*, 2854–2871. [CrossRef]
10. Alonso-Arroyo, A.; Zavorotny, V.U.; Camps, A. Sea Ice Detection Using U.K. TDS-1 GNSS-R Data. *IEEE Trans. Geosci. Remote Sens.* **2017**, *55*, 4989–5001. [CrossRef]
11. Yan, Q.; Huang, W. Spaceborne GNSS-R Sea Ice Detection Using Delay-Doppler Maps: First Results from the U.K. TechDemoSat-1 Mission. *IEEE J. Sel. Top. Appl. Earth Observ. Remote Sens.* **2016**, *9*, 4795–4801. [CrossRef]
12. Zhu, Y.; Tao, T.; Zou, J.; Yu, K.; Wickert, J.; Semmling, M. Spaceborne GNSS Reflectometry for Retrieving Sea Ice Concentration Using TDS-1 Data. *IEEE Geosci. Remote Sens. Lett.* **2020**, *18*, 612–616. [CrossRef]

13. Yan, Q.; Huang, W. Sea Ice Sensing From GNSS-R Data Using Convolutional Neural Networks. *IEEE Geosci. Remote Sens. Lett.* **2018**, *15*, 1510–1514. [CrossRef]
14. Yan, Q.; Huang, W. Sea Ice Thickness Measurement Using Spaceborne GNSS-R: First Results with TechDemoSat-1 Data. *IEEE J. Sel. Top. Appl. Earth Observ. Remote Sens.* **2020**, *13*, 577–587. [CrossRef]
15. Yan, Q.; Huang, W. Tsunami Detection and Parameter Estimation From GNSS-R Delay-Doppler Map. *IEEE J. Sel. Top. Appl. Earth Observ. Remote Sens.* **2016**, *9*, 4650–4659. [CrossRef]
16. Warnock, A.M.; Ruf, C.S.; Morris, M. Storm surge prediction with cygnss winds. In Proceedings of the 2017 IEEE International Geoscience and Remote Sensing Symposium (IGARSS), Fort Worth, TX, USA, 23–28 July 2017; pp. 2975–2978.
17. Li, X.; Yang, D.; Han, G.; Yang, L.; Wang, J.; Yang, J.; Chen, D.; Zheng, G. Exploiting the Potential of Coastal GNSS-R for Improving Storm Surge Modeling. *IEEE Geosci. Remote Sens. Lett.* **2021**, *18*, 1134–1138. [CrossRef]
18. Peng, Q.; Jin, S. Significant Wave Height Estimation from Space-Borne Cyclone-GNSS Reflectometry. *Remote Sens.* **2019**, *11*, 584. [CrossRef]
19. Yang, S.; Jin, S.; Jia, Y.; Ye, M. Significant Wave Height Estimation from Joint CYGNSS DDMA and LES Observations. *Sensors* **2021**, *21*, 6123. [CrossRef]
20. Bu, J.; Yu, K. Significant Wave Height Retrieval Method Based on Spaceborne GNSS Reflectometry. *IEEE Geosci. Remote Sens. Lett.* **2022**, *19*, 1503705. [CrossRef]
21. Bu, J.; Yu, K. A New Integrated Method of CYGNSS DDMA and LES Measurements for Significant Wave Height Estimation. *IEEE Geosci. Remote Sens. Lett.* **2022**, *19*, 1505605. [CrossRef]
22. Wang, F.; Yang, D.; Yang, L. Retrieval and Assessment of Significant Wave Height from CYGNSS Mission Using Neural Network. *Remote Sens.* **2022**, *14*, 3666. [CrossRef]
23. Yu, K.; Han, S.; Bu, J.; An, Y.; Zhou, Z.; Wang, C.; Tabibi, S.; Cheong, J.W. Spaceborne GNSS Reflectometry. *Remote Sens.* **2022**, *14*, 1605. [CrossRef]
24. Bu, J.; Yu, K.; Park, H.; Huang, W.; Han, S.; Yan, Q.; Qian, N.; Lin, Y. Estimation of Swell Height Using Spaceborne GNSS-R Data from Eight CYGNSS Satellites. *Remote Sens.* **2022**, *14*, 4634. [CrossRef]
25. Asgarimehr, M.; Zavorotny, V.; Wickert, J.; Reich, S. Can GNSS Reflectometry Detect Precipitation Over Oceans? *Geophys. Res. Lett.* **2018**, *45*, 12585–12592. [CrossRef]
26. Bu, J.; Yu, K.; Ni, J.; Yan, Q.; Han, S.; Wang, J.; Wang, C. Machine learning-based methods for sea surface rainfall detection from CYGNSS delay-doppler maps. *GPS Solut.* **2022**, *26*, 132. [CrossRef]
27. Bu, J.; Yu, K. Sea Surface Rainfall Detection and Intensity Retrieval Based on GNSS-Reflectometry Data from the CYGNSS Mission. *IEEE Trans. Geosci. Remote Sens.* **2022**, *60*, 5802015. [CrossRef]
28. Bu, J.; Yu, K.; Han, S.; Qian, N.; Lin, Y.; Wang, J. Retrieval of Sea Surface Rainfall Intensity Using Spaceborne GNSS-R Data. *IEEE Trans. Geosci. Remote Sens.* **2022**, *60*, 5803116. [CrossRef]
29. Yan, Q.; Huang, W.; Jin, S.; Jia, Y. Pan-tropical soil moisture mapping based on a three-layer model from CYGNSS GNSS-R data. *Remote Sens. Environ.* **2020**, *247*, 111944. [CrossRef]
30. Carreno-Luengo, H.; Luzi, G.; Crosetto, M. Above-Ground Biomass Retrieval over Tropical Forests: A Novel GNSS-R Approach with CyGNSS. *Remote Sens.* **2020**, *12*, 29. [CrossRef]
31. Clarizia, M.P.; Ruf, C.S.; Jales, P.; Gommenginger, C. Spaceborne GNSS-R Minimum Variance Wind Speed Estimator. *IEEE Trans. Geosci. Remote Sens.* **2014**, *52*, 6829–6843. [CrossRef]
32. Ruf, C.S.; Gleason, S.; McKague, D.S. Assessment of CYGNSS Wind Speed Retrieval Uncertainty. *IEEE J. Sel. Top. Appl. Earth Observ. Remote Sens.* **2019**, *12*, 87–97. [CrossRef]
33. Clarizia, M.P.; Ruf, C.S. Wind Speed Retrieval Algorithm for the Cyclone Global Navigation Satellite System (CYGNSS) Mission. *IEEE Trans. Geosci. Remote Sens.* **2016**, *54*, 4419–4432. [CrossRef]
34. Rodriguez-Alvarez, N.; Garrison, J.L. Generalized Linear Observables for Ocean Wind Retrieval from Calibrated GNSS-R Delay–Doppler Maps. *IEEE Trans. Geosci. Remote Sens.* **2016**, *54*, 1142–1155. [CrossRef]
35. Hammond, M.L.; Foti, G.; Rawlinson, J.; Gommenginger, C.; Srokosz, M.; King, L.; Unwin, M.; Roselló, J. First Assessment of Geophysical Sensitivities from Spaceborne Galileo and BeiDou GNSS-Reflectometry Data Collected by the UK TechDemoSat-1 Mission. *Remote Sens.* **2020**, *12*, 2927. [CrossRef]
36. Liu, Y.; Collett, I.; Morton, Y.J. Application of Neural Network to GNSS-R Wind Speed Retrieval. *IEEE Trans. Geosci. Remote Sens.* **2019**, *57*, 9756–9766. [CrossRef]
37. Asgarimehr, M.; Zhelavskaya, I.; Foti, G.; Reich, S.; Wickert, J. A GNSS-R Geophysical Model Function: Machine Learning for Wind Speed Retrievals. *IEEE Geosci. Remote Sens. Lett.* **2020**, *17*, 1333–1337. [CrossRef]
38. Reynolds, J.; Clarizia, M.P.; Santi, E. Wind Speed Estimation from CYGNSS Using Artificial Neural Networks. *IEEE J. Sel. Top. Appl. Earth Observ. Remote Sens.* **2020**, *13*, 708–716. [CrossRef]
39. Chu, X.; He, J.; Song, H.; Qi, Y.; Sun, Y.; Bai, W.; Li, W.; Wu, Q. Multimodal Deep Learning for Heterogeneous GNSS-R Data Fusion and Ocean Wind Speed Retrieval. *IEEE J. Sel. Top. Appl. Earth Observ. Remote Sens.* **2020**, *13*, 5971–5981. [CrossRef]
40. Asgarimehr, M.; Arnold, C.; Weigel, T.; Ruf, C.; Wickert, J. GNSS reflectometry global ocean wind speed using deep learning: Development and assessment of CyGNSSnet. *Remote Sens. Environ.* **2022**, *269*, 112801. [CrossRef]
41. Guo, W.; Du, H.; Guo, C.; Southwell, B.J.; Cheong, J.W.; Dempster, A.G. Information fusion for GNSS-R wind speed retrieval using statistically modified convolutional neural network. *Remote Sens. Environ.* **2022**, *272*, 112934. [CrossRef]

42. Li, X.; Yang, D.; Yang, J.; Zheng, G.; Han, G.; Nan, Y.; Li, W. Analysis of coastal wind speed retrieval from CYGNSS mission using artificial neural network. *Remote Sens. Environ.* **2021**, *260*, 112454. [CrossRef]
43. Liu, X.; Bai, W.; Xia, J.; Huang, F.; Yin, C.; Sun, Y.; Du, Q.; Meng, X.; Liu, C.; Hu, P.; et al. FA-RDN: A Hybrid Neural Network on GNSS-R Sea Surface Wind Speed Retrieval. *Remote Sens.* **2021**, *13*, 4820. [CrossRef]
44. Gleason, S. Space-Based GNSS Scatterometry: Ocean Wind Sensing Using an Empirically Calibrated Model. *IEEE Trans. Geosci. Remote Sens.* **2013**, *51*, 4853–4863. [CrossRef]
45. Gleason, S.; Ruf, C.S.; Clarizia, M.P.; Brien, A.J.O. Calibration and Unwrapping of the Normalized Scattering Cross Section for the Cyclone Global Navigation Satellite System. *IEEE Trans. Geosci. Remote Sens.* **2016**, *54*, 2495–2509. [CrossRef]
46. Jing, C.; Yang, X.; Ma, W.; Yu, Y.; Dong, D.; Li, Z.; Xu, C. Retrieval of sea surface winds under hurricane conditions from GNSS-R observations. *Acta Oceanol. Sin.* **2016**, *35*, 91–97. [CrossRef]
47. Bu, J.; Yu, K.; Zhu, Y.; Qian, N.; Chang, J. Developing and Testing Models for Sea Surface Wind Speed Estimation with GNSS-R Delay Doppler Maps and Delay Waveforms. *Remote Sens.* **2020**, *12*, 3760. [CrossRef]
48. Clarizia, M.P.; Ruf, C.S. Statistical Derivation of Wind Speeds from CYGNSS Data. *IEEE Trans. Geosci. Remote Sens.* **2020**, *58*, 3955–3964. [CrossRef]
49. Clarizia, M.P.; Ruf, C.S. Bayesian Wind Speed Estimation Conditioned on Significant Wave Height for GNSS-R Ocean Observations. *J. Atmos. Ocean. Technol.* **2017**, *34*, 1193–1202. [CrossRef]
50. Wang, C.; Yu, K.; Qu, F.; Bu, J.; Han, S.; Zhang, K. Spaceborne GNSS-R Wind Speed Retrieval Using Machine Learning Methods. *Remote Sens.* **2022**, *14*, 3507. [CrossRef]
51. Li, C.; Huang, W. An Algorithm for Sea-Surface Wind Field Retrieval From GNSS-R Delay-Doppler Map. *IEEE Geosci. Remote Sens. Lett.* **2014**, *11*, 2110–2114. [CrossRef]
52. Foti, G.; Gommenginger, C.; Jales, P.; Unwin, M.; Shaw, A.; Robertson, C.; Rosello, J. Spaceborne GNSS reflectometry for ocean winds: First results from the UK TechDemoSat-1 mission. *Geophys. Res. Lett.* **2015**, *42*, 5435–5441. [CrossRef]
53. Bu, J.; Yu, K.; Han, S.; Wang, C. Multi-Observable Wind Speed Retrieval Based on Spaceborne GNSS-R Delay Doppler Maps. In Proceedings of the IGARSS 2021-2021 IEEE International Geoscience and Remote Sensing Symposium, Brussels, Belgium, 11–16 July 2021; pp. 7580–7583.
54. Ruf, C.S.; Balasubramaniam, R. Development of the CYGNSS Geophysical Model Function for Wind Speed. *IEEE J. Sel. Top. Appl. Earth Observ. Remote Sens.* **2019**, *12*, 66–77. [CrossRef]
55. Guo, W.; Du, H.; Cheong, J.W.; Southwell, B.J.; Dempster, A.G. GNSS-R Wind Speed Retrieval of Sea Surface Based on Particle Swarm Optimization Algorithm. *IEEE Trans. Geosci. Remote Sens.* **2022**, *60*, 4202414. [CrossRef]
56. Atlas, R.; Hoffman, R.N.; Ardizzone, J.; Leidner, S.M.; Jusem, J.C.; Smith, D.K.; Gombos, D. A cross-calibrated, multiplatform ocean surface wind velocity product for meteorological and oceanographic applications. *Bull. Am. Meteorol. Soc.* **2011**, *92*, 157–174. [CrossRef]
57. Mears, C.A.; Scott, J.; Wentz, F.J.; Ricciardulli, L.; Leidner, S.M.; Hoffman, R.; Atlas, R. A near-real-time version of the cross-calibrated multiplatform (CCMP) ocean surface wind velocity data set. *J. Geophys. Res. Ocean.* **2019**, *124*, 6997–7010. [CrossRef]
58. Marchan-Hernandez, J.F.; Valencia, E.; Rodriguez-Alvarez, N.; Ramos-Perez, I.; Bosch-Lluis, X.; Camps, A.; Eugenio, F.; Marcello, J. Sea-State Determination Using GNSS-R Data. *IEEE Geosci. Remote Sens. Lett.* **2010**, *7*, 621–625. [CrossRef]
59. Zhu, Y.; Yu, K.; Zou, J.; Wickert, J. Sea Ice Detection Based on Differential Delay-Doppler Maps from UK TechDemoSat-1. *Sensors* **2017**, *17*, 1614. [CrossRef]
60. Said, F.; Jelenak, Z.; Park, J.; Soisuvarn, S.; Chang, P.S. A 'track-wise' wind retrieval algorithm for the CYGNSS mission. In Proceedings of the IGARSS 2019-2019 IEEE International Geoscience and Remote Sensing Symposium, Yokohama, Japan, 28 July–2 August 2019; pp. 8711–8714.
61. Said, F.; Jelenak, Z.; Park, J.; Chang, P.S. The NOAA Track-Wise Wind Retrieval Algorithm and Product Assessment for CyGNSS. *IEEE Trans. Geosci. Remote Sens.* **2022**, *60*, 4202524. [CrossRef]
62. Balasubramaniam, R.; Ruf, C. Characterization of rain impact on L-Band GNSS-R ocean surface measurements. *Remote Sens. Environ.* **2020**, *239*, 111607. [CrossRef]
63. Ertuğrul, Ö.F. A novel type of activation function in artificial neural networks: Trained activation function. *Neural Netw.* **2018**, *99*, 148–157. [CrossRef]
64. Saïd, F.; Katzberg, S.J.; Soisuvarn, S. Retrieving hurricane maximum winds using simulated CYGNSS power-versus-delay waveforms. *IEEE J. Sel. Top. Appl. Earth Observ. Remote Sens.* **2017**, *10*, 3799–3809. [CrossRef]
65. Ruf, C.; Unwin, M.; Dickinson, J.; Rose, R.; Rose, D.; Vincent, M.; Lyons, A. CYGNSS: Enabling the Future of Hurricane Prediction [Remote Sensing Satellites]. *IEEE Geosci. Remote Sens. Mag.* **2013**, *1*, 52–67. [CrossRef]
66. Wang, X.; Shum, C.; Johnson, J. Analysis of Surface Wind Diurnal Cycles in Tropical Regions using Mooring Observations and the CCMP Product. In Proceedings of the Conference on Hurricanes and Tropical Meteorology American Meteorological Society, Washington, DC, USA, 1–4 April 2014; p. 7A.7.
67. Li, X.; Yang, D.; Yang, J.; Han, G.; Zheng, G.; Li, W. Validation of NOAA CyGNSS Wind Speed Product with the CCMP Data. *Remote Sens.* **2021**, *13*, 1832. [CrossRef]
68. Dong, Z.; Jin, S. Evaluation of Spaceborne GNSS-R Retrieved Ocean Surface Wind Speed with Multiple Datasets. *Remote Sens.* **2019**, *11*, 2747. [CrossRef]

69. Tianyu, Z.; Zhenjiang, M.; Jianhu, Z. Combining cnn with hand-crafted features for image classification. In Proceedings of the 2018 14th IEEE International Conference on Signal Processing (ICSP), Beijing, China, 12–16 August 2018; pp. 554–557.
70. Zhang, S.; Li, C.; Qiu, S.; Gao, C.; Zhang, F.; Du, Z.; Liu, R. EMMCNN: An ETPS-Based Multi-Scale and Multi-Feature Method Using CNN for High Spatial Resolution Image Land-Cover Classification. *Remote Sens.* **2020**, *12*, 66. [CrossRef]
71. Nabi, M.; Senyurek, V.; Gurbuz, A.C.; Kurum, M. Deep Learning-Based Soil Moisture Retrieval in CONUS Using CYGNSS Delay–Doppler Maps. *IEEE J. Sel. Top. Appl. Earth Observ. Remote Sens.* **2022**, *15*, 6867–6881. [CrossRef]
72. Zeng, L.; Brown, R.A. Scatterometer observations at high wind speeds. *J. Appl. Meteorol.* **1998**, *37*, 1412–1420. [CrossRef]
73. Querol, J.; Alonso-Arroyo, A.; Onrubia, R.; Pascual, D.; Park, H.; Camps, A. SNR degradation in GNSS-R measurements under the effects of radio-frequency interference. *IEEE J. Sel. Top. Appl. Earth Observ. Remote Sens.* **2016**, *9*, 4865–4878. [CrossRef]
74. Asgarimehr, M.; Wickert, J.; Reich, S. TDS-1 GNSS reflectometry: Development and validation of forward scattering winds. *IEEE J. Sel. Top. Appl. Earth Observ. Remote Sens.* **2018**, *11*, 4534–4541. [CrossRef]